Dissertação de Mestrado

Inatel
Instituto Nacional de Telecomunicações

Low complexity Sub-optimal GFDM Receiver for Remote Areas

WHEBERTH DAMASCENA DIAS

JULY 2021

SUB-OPTIMAL LOW COMPLEXITY GFDM RECEIVER FOR REMOTE AREAS

WHEBERTH DAMASCENA DIAS

This thesis was presented at Inatel, as part of the requirements for obtaining a Master's Degree in Telecommunications.

ADVISOR: Prof. Dr. Luciano Leonel Mendes.

Santa Rita do Sapucaí
2021

Dias, Wheberth Damascena
D541l
Low complexity Sub-optimal GFDM Receiver for Remote Áreas. / Wheberth Damascena Dias – Santa Rita do Sapucaí, 2021.
70p.

Orientador: Prof. Dr. Luciano Leonel Mendes.
Dissertação de Mestrado em Telecomunicações – Instituto Nacional de Telecomunicações – INATEL.
Inclui bibliografia.

1. Equalização 2. GFDM 3. MMSE 4. ZF 5. Software Defined Radio 6. Mestrado em Telecomunicações. I. Mendes, Luciano Leonel. II. Instituto Nacional de Telecomunicações – INATEL. III. Título.

CDU 621.39

Ficha Catalográfica elaborada pelo Bibliotecário da Instituição
CRB6-2718 – Paulo Eduardo de Almeida

APPROVAL FORM

Dissertação defendida e aprovada em _____/_____/_____, pela comissão julgadora:

Prof. Dr. Luciano Leonel Mendes
INATEL

Dr. Henry Douglas Rodrigues
INATEL

Prof. Dr. Paulo Cardieri
UNICAMP

Coordenador do Curso de Mestrado
Prof. Dr. José Marcos Camara Brito

“The day you stop learning, is when you start dying”

Albert Einstein

Aos meus pais,
meus primeiros grandes professores.

Acknowledgments

Throughout my academic journey, I had received a big amount of support and encouragement that were fundamental to drive me towards this accomplishment. This cooperation came in the most diverse forms such as advice, technical knowledge, comprehension, and constructive critics. I am very grateful for every single human interaction I had during the course of my studies.

First, I would thank my supervisor, Professor Dr. Luciano L. Mendes who shed light on my path sparking my curiosity and encouraging me to always look beyond the ordinary. I also would like to thank you, and all the Master's program coordinators for your patience and comprehension during the writing of this thesis.

I would like to thank the Finatel institution for the scholarship to the Master's program and the opportunity to work in an environment that inspires and support creativity, driving technological innovation all the way, from research to the industry.

I also thank all my colleagues at the Radiocommunications Reference Center (CRR) and the 5G Range project team for all our technical and personal exchanges in such a pleasant research environment and all time together on the lab and presentations.

I would like to thank my wife Lanuza, for all the support, incentive, and comprehension, during the uncountable hours of my physical and, sometimes, mental absence. I can't forget to thank my daughter Maria Luiza, for her ability to break a smile even on the most serious faces after a long and exhaustive day.

I would like to dedicate this thesis to my parents, Pedro and Maria Marta, and thank them for all their efforts to raise and educate, me and my brothers, not only providing us access to schools and books but particularly being such great examples.

Wheberth Damascena Dias

Summary

List of Figures

List of Tables

Abbreviations

1G	First Generation
2G	Second Generation
3G	Third Generation
3GPP	The 3rd Generation Partnership Project
4G	Fourth Generation
5G	Fifth Generation
AMMSE	Low-rank Approximated MMSE Receiver
ARM	Advanced RISC Machines
ASIC	Application Specific Integrated Circuit
AVX2	Advanced Vector Extensions 2
AWGN	Additive White Gaussian Noise
CIR	Channel Impulse Response
CM	Complex-valued multiplication
CP	Cyclic Prefix
CPU	Central Processing Unit
CR	Cognitive Radio
CSI	Channel State Information
DFT	Discrete Fourier Transform
DSP	Digital Signal Processing
eMBB	Enhanced mobile broadband
FDE	Frequency-Domain Equalizer
FDM	Frequency Division Multiplexing
FFT	Fast Fourier Transform
FFTW	Fastest Fourier Transformer in the West
FIR	Finite Impulse Response
F-OFDM	Filtered OFDM
FPGA	Field-Programmable Gate Array
FSC	Frequency Selective Channel
GCC	GNU C Compiler
GFDM	Generalized Frequency Division Multiplexing
GPP	General-Purpose Processor
IBI	Inter-Block Interference
IDFT	Inverse Discrete Fourier Transform
IFFT	Inverse Fast Fourier Transform
IMT	International Mobile Telecommunications
IoT	Internet of Things

IP	Internet Protocol
ISP	Internet Service Provider
ITU	International Telecommunications Union
LDGT	Local Discrete Gabor Transform
LTE	Long-Term Evolution
MAC	Media Access Control
MF	Matched Filter
MIMO	Multiple-Input/Multiple-Output
MMSE	Minimum Mean Square Error
MSE	Mean Square Error
MTC	Machine-type communications
NLoS	Non Line-of-Sight
OFDM	Orthogonal Frequency Division Multiplexing
OOB	Out-of-Band
OpenMP	Open Multi-Processing
PHY	Physical Layer
PU	Primary User
QAM	Quadrature and Amplitude Modulation
RB	Resource Block
SDR	Software Defined Radio
SER	Symbol Error Rate
SFN	Single-Frequency Network
SIMD	Single Instruction Multiple Data
SISO	Single-Input/Single-Output
STBC	Space-Time Block coding
SU	Secondary User
TR-STBC	Time-reversed Space-Time Block Coding
TV	Television
TVWS	TV White Space
UHF	Ultra-High Frequency
URLLC	Ultra reliable low-latency communications
VHF	Very-High Frequency
W-OFDM	Windowed OFDM
ZF	Zero-Forcing

List of Symbols

$\mathbf{A}$	GFDM Transmit matrix
$\mathbf{B}$	GFDM Receiver matrix
$\mathcal{O}(\cdot)$	Complexity in big-$\mathcal{O}$ notation
$\mathcal{C}_{\mathrm{P}_{\mathrm{FFT}}}$	Computational complexity in number of CMs
$\circledast$	Circular convolution operator
d_k	QAM symbol modulating the k-th subcarrier
$d_{k,m}$	QAM symbol modulating the k-th subcarrier at the m-th subsymbol
$\mathbf{d}$	Complex-valued information symbols to be transmitted
$\mathrm{E}\{\cdot\}$	Statistical expectation operator, denotes the expected value of a random variable
$\boldsymbol{\mathcal{F}}_{\langle K \rangle}$	Normalized Fourier matrix of order K
$\mathbf{H}$	Circulant channel matrix
$(\cdot)^{\mathrm{H}}$	Hermitian operator, denotes the transposition of a matrix and complex-conjugation of its elements
$\mathscr{F}^{-1}$	Inverse discrete Fourier transform
j	The imaginary number equals to $\sqrt{-1}$
k	Subcarrier index
K	Number of subcarriers
m	Subsymbol index
M	Number of subsymbols
n	Discrete time or sample index
$\Vert \cdot \Vert_2$	ℓ^2-norm
$\mathbf{w}$	AWGN noise vector
$x^K_{(\mathrm{OFDM})}$	Baseband OFDM signal with K subcarriers in time-domain
$\mathbf{x}$	Signal vector composed by the discrete time-domain samples $[x_0, x_1, x_2, \ldots, x_{(K-1)}]^{\mathrm{T}}$

Abstract

Dias, Wheberth. *"Low complexity Sub-optimal GFDM Receiver for Remote Areas"* [master's thesis]. Santa Rita do Sapucaí: Instituto Nacional de Telecomunicações; 2021.

Generalized Frequency Division Multiplexing (GFDM) is a waveform, initially proposed for 5G, that can play an important role in some applications. It offers low out-of-band emission, good spectral efficiency and has the flexibility to cover the 5G requirements in remote area scenarios. The GFDM receiver implementation complexity poses restrictions to the use of this powerful waveform in constrained resources devices, such as the ones used in Internet of Things (IoT). This thesis proposes, a sub-optimal receiver chain using frequency-domain equalization, offering a complexity comparable to the Zero-Forcing (ZF) receiver while achieving performance close to the Minimum Mean Square Error (MMSE) receiver. The study also evaluates the proposed equalizer performance under frequency selective fading channel for the Single-Input/Single-Output (SISO) and Multiple-Input/Multiple-Output (MIMO) cases. Simulation results show that with a small increment in complexity, in comparison with ZF, a performance gain in Symbol Error Rate (SER) can be obtained. An implementation of the proposed chain using the Software Defined Radio (SDR) approach, suggests that the proposed scheme is feasible for practical real-time deployments.

***Keyords*:** GFDM, Equalization, Software Defined Radio

Resumo

Dias, Wheberth. *"Low complexity Sub-optimal GFDM Receiver for Remote Areas"*, [dissertação de mestrado]. Santa Rita do Sapucaí: Instituto Nacional de Telecomunicações; 2021.

GFDM é uma forma de onda, inicialmente proposta para o 5G, que pode desempenhar um papel importante em diversas aplicações. Ela oferece baixa emissão fora da faixa, boa eficiência espectral e oferece flexibilidade para cobrir os requisitos do 5G em cenários de área remota. A complexidade de implementação do receptor GFDM impõe restrições ao uso desta poderosa forma de onda em dispositivos com recursos restritos, como os usados em IoT. Esta tese propõe uma cadeia de recepção sub-ótima usando equalização no domínio da frequência, oferecendo uma complexidade comparável à do receptor ZF, enquanto se obtém um desempenho próximo ao do receptor MMSE. O estudo também avalia o desempenho sistema proposto em canal com desvanecimento seletivo em frequência para os casos SISO e MIMO. Os resultados das simulações mostram que, com um pequeno acréscimo de complexidade, em comparação com o ZF, é possível obter um ganho de desempenho na SER. Uma implementação da cadeia proposta, utilizando a abordagem SDR, sugere que este esquema é viável para implementação em sistemas de comunicação práticos.

***Palavras-Chave*:** GFDM, Equalização, Radio definido por software

Chapter 1

Introduction

THE cellular mobile communications systems were born in the 80s. The frequency reuse allowed the efficient use of the spectrum and made it possible to offer the service on a large scale. Back in those days, the main feature of the First Generation (1G) cellular networks was mobility. The user no longer needed to be connected to the central office by a copper wire to make or receive voice calls [1].

The Second Generation (2G) of the mobile communication systems was introduced at the end of the 80s and employed digital communications and voice compression techniques to overcome interference and make even more efficient use of the spectrum, further expanding the offer of the service. The 2G had improved the voice quality and allowed the users to exchange text messages [1]. The so-called 2.5G systems were able to deliver up to 144 kilobits per second of data throughput.

With the Third Generation (3G), the main focus of the mobile networks started to change from voice calls to data transmission. The network was hybrid and still employing circuit switching techniques for voice calls, and packet switching for data traffic. The strong growth in the adoption of the smartphone, along with increased data rates, caused a significant boost on the user experience concerning mobile Internet access.

The next generation of mobile networks, the Fourth Generation (4G), has abolished the circuit switching completely and embraced Internet Protocol (IP) connectivity as its main service. The Long-Term Evolution (LTE)-Advanced standard from The 3rd Generation Partnership Project (3GPP) fullfils the requirements of the International Mobile Telecommunications (IMT) Advanced, offering peak data rates up to 100 Mbps for mobile users. The 4G also introduced the Orthogonal Frequency Division Multiplexing (OFDM) waveform supporting the use of multiple antenna techniques increasing even more the spectral efficiency achieved by mobile networks, and improving radio resources allocation compared with previous technologies.

By the introduction of the 4G, mobile connectivity had become an essential part of people's everyday life. With Fifth Generation (5G), the role of connectivity is expected to be even more important. The data throughput is expected to achieve ten-fold over the previous technology at the users' mobile phones, although this is not the most important feature of this generation of mobile systems. The 5G has been developed with the focus on three main features, namely: enhanced mobile broadband (eMBB) con-

nectivity, machine-type communications (MTC), and ultra reliable low-latency communications (URLLC). The envisioned applications scenarios for these features leads to an unprecedented level of automation ranging from having wearable devices, such as clothes and shoes connected to the internet, to self-driving cars and industrial plants controlled by services and resources hosted on the cloud.

To offer such high bandwidth, the 5G networks use large portions of spectrum bands available at frequency bands over 6 GHz and extending up to 41 GHz. The propagation loss related to such high frequencies requires a dense network with a smaller cell diameter. While this approach is suitable for urban areas and, particularly attractive for metropolitan regions, it does not provide a solution for large areas with a low-density population [2].

Despite the evolution of the mobile wireless networks, the International Telecommunications Union (ITU) estimated, by the end of 2019, that 3.6 billion people still are unconnected [3]. Part of this population is located in remote and sparsely populated areas and may not benefit directly from the proposed main use case scenarios for 5G network deployment and remain unconnected.

Recent studies [4, 5] found evidence that the adoption of information and communication technologies, such as mobile phone and broadband Internet adoption, plays a positive and significant role as drivers of economic growth. Connectivity can also expand the use of technology on farms, increasing the efficiency of plantation crops, reducing the need for natural resources, such as water and land. Precision agriculture can reduce the volume of pesticides employed in plantations, also affecting positively the environment.

The lack of connectivity is a real problem and, over the last decade, is possible to observe many initiatives to tackle this issue coming from academia, government, and the private sector. To name a few we can cite Google's Loon [6], Facebook's Aquila and Telecom Infra projects, and SpaceX's Starlink.

It is clear that Internet connectivity can bring benefits to remote and low population density areas. The evolution of the standards for mobile networks alone does not improve the situation in remote areas and the current technologies don't provide a cost-effective solution to turn the underserved areas into profitable markets.

The research object of this master thesis was partially developed under the context of 5G-Range project, whose main goal was to propose a solution for cost-effective connectivity in remote areas. The 5G-Range project proposes the use of the left over spectrum from the digitization of Broadcast television, combined with efficient and robust communication techniques, such as Generalized Frequency Division Multiplexing (GFDM) waveform and Multiple-Input/Multiple-Output (MIMO) for diversity [7, 8]. Using this approach the cost related to spectrum licenses can be reduced and, at the same time, the area covered by a base station can be extended. As a result, the research and technology selection presented in this thesis reflects partially the goals pursued by that project. Despite this fact is important to emphasize that the proposed scheme is not limited to the reference applications scenario.

1.1 Contribution and Prior Work

GFDM is an attractive waveform that was initially proposed for the physical layer of the 5G. However, the complexity of the Minimum Mean Square Error (MMSE) GFDM receiver is high and needs to be addressed in order to allow the advantages proposed by this waveform to be fully exploited in practical real-time implementations. Many researchers have contributed with the development of this waveform. In [9], the authors used the frequency sparsity of some pulse formats to propose a low complexity architecture. The authors in [10] proposed complexity reduction in transmitter and receiver based on block diagonal property of the GFDM transmit matrix.

Nevertheless, only Matched Filter (MF) and Zero-Forcing (ZF) receivers are addressed for the Frequency Selective Channel (FSC) that, in fact, encompasses most of the practical wireless communication systems. In [11], the authors also exploit block circularity property of the GFDM transmit matrix to achieve the complexity reduction of the MMSE, once again, assuming FSC. The authors in [12] proposed an approximate MMSE solution with complexity of $\mathcal{O}(N \log N)$, called Local Discrete Gabor Transform (LDGT) solution. In [13], the authors also achieved the same complexity with the Low-rank Approximated MMSE Receiver (AMMSE) solution.

This work proposes a new receiver structure for GFDM, where a trade-off between complexity and performance is achieved. The Symbol Error Rate (SER) performance of the proposed receiver over FSC is analyzed and compared with other linear receivers available for GFDM. The complexity of the proposed scheme is also considered in this work. The design of this GFDM receiver structure and its key performance analysis are original contributions of this master's thesis. Finally, this work brings a Software Defined Radio (SDR) implementation of the proposed algorithm, showing that it can be used for real-time systems.

The remaining of this thesis is organized as follows: Chapter 2 provides background information on the GFDM waveform. The OFDM have inspired the development of many multi-carrier waveforms, including GFDM. It is used in many wireless standards and practical systems. For this reason it is also briefly introduced and used as a reference through this thesis. Also in Chapter 2, the main characteristics that makes those waveforms relevant for remote areas applications are presented along with the computational complexity of both. Chapter 2 also introduces the Space-Time Block coding (STBC) MIMO technique and a Low-complexity implementation of the GFDM waveform.

Chapter 3 describes the proposed receiver chain and the reasoning underlying the proposal. The analysis of the resulting complexity is presented along with its SER performance evaluation.

Chapter 4 describes a real-time SDR implementation of the proposed scheme written in C and C++ language and shows the achieved sample rate.

Chapter 5 presents the conclusions and final considerations of this thesis.

Chapter 2

Background and Fundamentals

Due to a diminishing availability of spectrum bandwidth, the evolution of wireless communication systems requires efficient use and exploitation of any vacant spectrum. The Physical Layer (PHY) and Media Access Control (MAC) layer must employ techniques that allow the fragmented and dynamic spectrum allocation of the available bands as a secondary unlicensed network, protecting the Primary Users (PUs). This chapter presents essential techniques and waveforms that allow this exploitation.

2.1 Motivations for TV White Spaces Exploitation

The portion of the spectrum assigned for broadcast television covers the frequency range located from 174 MHz to 230 MHz, in the Very-High Frequency (VHF) band, and between 470 MHz and 698 MHz, in the Ultra-High Frequency (UHF) band, with channels bandwidths of 6, 7 or 8 MHz, depending on the frequency band and country. Combined, these two bands comprise 284 MHz worth of spectrum. The analog television (TV) technology usually required a guard channel to mitigate interference between adjacent channels, leading to inefficient use of the spectrum, where many channels were left unused.

Digital TV broadcast standards, eliminates the need of a guard channel. This advance, in combination with other features, such as multi-programming, and Single-Frequency Networks (SFNs), allows the more efficient use of the spectrum. As a result, the transition from analog to digital TV broadcast has already released the portion of the spectrum, known as 700 MHz band, which is now designated for mobile broadband and denominated LTE Band 28. As the transition advances, more channels are expected to be freed.

The vacant TV channels are the so-called TV White Spaces (TVWSs), and they are candidates to be shared by Cognitive Radio (CR) based networks [14]. In the TVWS context, the PUs are the license owners, which are the TV broadcasters. The Secondary Users (SUs) are the ones that make opportunistic use of the spectrum when the PU is not present. The SUs, however, cannot cause harmful interference to the PU. This constraint requires some method to know about its presence, such as spectrum sensing and geographic databases. The Out-of-Band (OOB) emissions of the SU must

be strictly controlled in such a way that it does not cause interference on adjacent channels.

In remote and low populated areas, the occupancy of TV channels is sparse [15]. Furthermore, the range of frequencies below 1 GHz is well suited for Non Line-of-Sight (NLoS) propagation, making the use of TVWS very attractive for deploying secondary networks aiming to provide long-range coverage for sparsely populated areas. The exploitation of TVWS can reduce the costs associated with spectrum licensing and, combined with a modern regulatory framework, has the ability to bring Internet access to remote areas, reducing the number of unconnected people and enhancing the use of technology in agriculture.

2.2 OFDM Waveform

OFDM is a well-established waveform adopted by many wired and wireless communication standards due to its performance in multi-path environments, relatively simple transceiver implementation, and straightforward resource allocation management.

OFDM is a multi-carrier waveform, where the transmitter splits a block of information symbols among several narrowband and orthogonal subcarriers. As opposed to legacy Frequency Division Multiplexing techniques, no guard band is reserved in between the subcarriers, which overlap with each other but keeping the orthogonality due to the proper frequency spacing. This approach leads to efficient use of the spectrum.

The baseband OFDM symbol is defined as [16]

$$x_{\mathrm{OFDM}}[n] = \sum_{k=0}^{K-1} d_k \cdot e^{-\jmath(\frac{2\pi k}{K})n}, (n = 0, 1, 2, \ldots, K-1) \tag{2.1}$$

in which n is the discrete time index, k is the subcarrier index, K is the number of subcarriers and d_k is the complex-valued information symbol transmitted by the kth subcarrier.

This process is equivalent to take the Inverse Discrete Fourier Transform (IDFT) of the data, d_k and (2.1) can be rewritten as

$$x_{\mathrm{OFDM}}[n] = \mathscr{F}^{-1}\{\mathbf{d}\}. \tag{2.2}$$

Alternatively, the OFDM symbol can be described by matrix operations. In this case, the OFDM discrete time-domain signal vector $\mathbf{x}$ is obtained by the product

$$\mathbf{x} = \boldsymbol{\mathcal{F}}^{\mathrm{H}}\mathbf{d}, \tag{2.3}$$

in which the $\boldsymbol{\mathcal{F}}$ is the $(K \times K)$ normalized Discrete Fourier Transform (DFT) matrix [17]. The symbol $(\cdot)^{\mathrm{H}}$ denotes the Hermitian operation.

When the transmitted OFDM signal undergoes the channel, it convolves with the Channel Impulse Response (CIR). The thermal noise is added to the signal at the receiver's antenna. The linear convolution with the CIR causes Inter-Block Interference

(IBI) to the subsequent OFDM symbol. This effect can be avoided by inserting a cyclic extension in between the OFDM symbols, called Cyclic Prefix (CP). The condition is that the CIR is not longer than the CP duration. When this condition is met, the spreading caused by the linear convolution of one OFDM symbol with the CIR is contained within the CP of the next symbol. When the CP is removed at the receiver, no IBI occurs. Figure 2.1 depicts the spreading caused by the channel and shows how the CP prevents IBI. In Figure 2.1(b) the spreading caused by the convolution with the channel impulse response, overlaps the subsequent OFDM symbol. In Figure 2.1(c) the last samples of the OFDM symbol are copied to form the CP. Finally, Figure 2.1(d) shows how the spread overlaps only the CP at the beginning of the next symbol. As the CP is identical to last portion of the symbol, the result is equivalent to a circular convolution of the OFDM with the CIR.

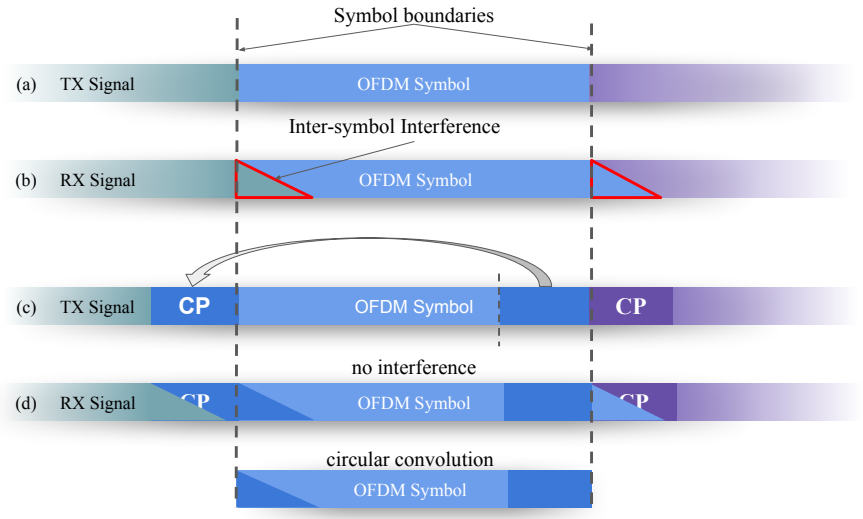

Figure 2.1: *CP insertion and IBI avoidance.*

After removing the CP, the received signal can be defined as

$$\mathbf{y} = \mathbf{H}\boldsymbol{\mathcal{F}}^{\mathrm{H}}\mathbf{d} + \mathbf{w}. \tag{2.4}$$

in which $\mathbf{H}$ is the $(K \times K)$ circulant channel matrix built from the CIR and the vector $\mathbf{w}$ is composed by the white noise samples in time-domain. The received signal in frequency domain is

$$\mathcal{Y} = \boldsymbol{\mathcal{F}}\mathbf{y} = \boldsymbol{\mathcal{F}}\mathbf{H}\boldsymbol{\mathcal{F}}^{\mathrm{H}}\mathbf{d} + \boldsymbol{\mathcal{F}}\mathbf{w}. \tag{2.5}$$

The data symbols can be estimated in frequency domain as

$$\hat{\mathbf{d}} = (\boldsymbol{\mathcal{F}}\mathbf{H}\boldsymbol{\mathcal{F}}^{\mathrm{H}})^{-\mathbf{1}}(\boldsymbol{\mathcal{F}}\mathbf{H}\boldsymbol{\mathcal{F}}^{\mathrm{H}})\mathbf{d} + (\boldsymbol{\mathcal{F}}\mathbf{H}\boldsymbol{\mathcal{F}}^{\mathrm{H}})^{-\mathbf{1}}\boldsymbol{\mathcal{F}}\mathbf{w}, \tag{2.6}$$

leading to

$$\hat{\mathbf{d}} = (\boldsymbol{\mathcal{F}}\mathbf{H}^{-1}\boldsymbol{\mathcal{F}}^{\mathrm{H}})(\boldsymbol{\mathcal{F}}\mathbf{H}\boldsymbol{\mathcal{F}}^{\mathrm{H}})\mathbf{d} + (\boldsymbol{\mathcal{F}}\mathbf{H}^{-\mathbf{1}}\boldsymbol{\mathcal{F}}^{\mathrm{H}})\mathbf{w}, \tag{2.7}$$

where the matrix $(\boldsymbol{\mathcal{F}}\mathbf{H}^{-1}\boldsymbol{\mathcal{F}}^{\mathrm{H}})$ is diagonal and the elements on its main diagonal are the reciprocal of the channel frequency response. Finally,

$$\hat{\mathbf{d}} = \mathbf{d} + (\boldsymbol{\mathcal{F}}\mathbf{H}^{-1}\boldsymbol{\mathcal{F}}^{\mathrm{H}})\mathbf{w}. \tag{2.8}$$

2.2.1 OFDM Cyclic prefix efficiency

The CP length is defined by the CIR, since the number of samples used to protect the symbol from IBI must the larger than the channel impulse response. For channels with long delay profiles, the CP can significantly impact the overall system performance, since it does not carry user data. The OFDM efficiency due to the CP is given by

$$\eta_{\mathrm{CP}} = \frac{K}{K + K_{\mathrm{CP}}} \times 100\%, \tag{2.9}$$

where the K_{CP} is CP length.

Figure 2.2 depicts an OFDM symbol with two different CP sizes. Figure 2.2a shows an OFDM symbol with a short CP that leads to an efficiency of 90%, and Figure 2.2b that shows a OFDM symbol with long CP achieving an efficiency of 66%.

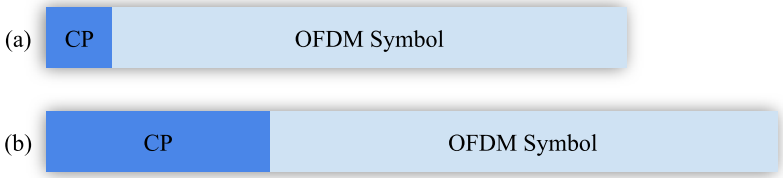

Figure 2.2: *OFDM symbol with two different CP length.*

2.2.2 OFDM Out-of-band emissions

At every OFDM symbol, the Quadrature and Amplitude Modulation (QAM) symbols modulating every subcarrier changes abruptly and this operation is equivalent to to modulate every subcarrier with a rectangular pulse in time domain. The spectrum of a rectangular pulse in the frequency domain is a $\mathrm{sinc(x)}$ function, which leads high OOB emissions. Figure 2.3 illustrates the OOB of the OFDM waveform. The sinc-shaped spectrum of individual subcarrier is shown along with the composite OFDM spectrum. The power spectral density of the OOB emissions approaches only 30 dB below the the in-band signal density [18].

The OOB emissions can cause harmful interference to other systems coexisting in adjacent frequencies. Without additional containment measures, this undesired effect can render the traditional OFDM waveform unsuitable for applications such as the opportunistic use of the spectrum in TVWS, which relies on the fact that the SU will not interfere with the the PU. Variations of the OFDM, such as the Filtered OFDM (F-OFDM) [19] and the Windowed OFDM (W-OFDM) [20] waveforms were developed to address this specific limitation. The F-OFDM employs a Finite Impulse Response (FIR) filtering process in order to attenuate the OOB emissions, while the W-OFDM employs a time windowing process aiming for smoothing the transition between two adjacent symbols.

2.3 GFDM Waveform

GFDM is a flexible non-orthogonal waveform proposed for the 5G PHY layer.

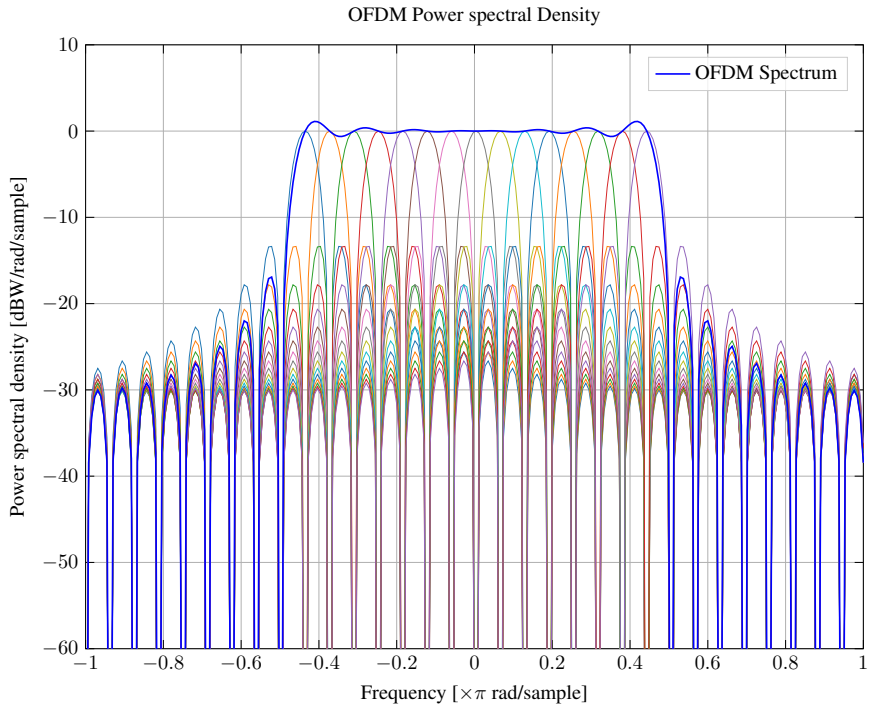

Figure 2.3: *Power spectrum density for individual OFDM subcarriers and for all subcarriers.*

In GFDM, every individual subcarrier is pulse-shaped to allow OOB emissions control [21]. As its name implies, GFDM is a generalized framework able to describe many waveforms, including OFDM. It allows for more flexibility on the waveform construction to achieve desired characteristics. The GFDM symbol is composed by M subsymbols that are cyclic time-shifted versions of the prototype filter kernel $g_0[n]$, weighted by the complex-valued information symbols to be carried. Each one of the K subcarriers is a cyclic frequency-shifted version of the prototype filter.

The time-domain GFDM waveform symbol is given by

$$x[n] = \sum_{k=0}^{K-1} \sum_{m=0}^{M-1} d_{k,m} \cdot g_0[\langle n - mK \rangle_N] \cdot \exp\left(\jmath 2\pi \frac{k}{K} n\right), \tag{2.10}$$

where $d_{k,m}$ is the complex-valued data symbol to be transmitted at the kth subcarrier and mth subsymbol. The prototype filter g_0 is composed by $N = KM$ samples and the $\langle \cdot \rangle_N$ denotes a modulo N operation.

While the OFDM sinc-shaped spectrum leads in orthogonality between the subcarriers, this is not guaranteed in GFDM and it will depend on the prototype filter selection. Interaction between adjacent subcarriers and subsymbols can occur, resulting in a non-orthogonal system.

As opposed to the OFDM waveform, the transmission pulse of the GFDM waveform can be designed to allow shaping of the spectrum of the subcarriers, reducing OOB significantly. Table 2.1 shows the expression of common GFDM transmission pulses, where

$$\text{lin}_\alpha(x) = \min\left(1, \max\left(0, \frac{1+\alpha}{2\alpha} + \frac{|x|}{\alpha}\right)\right) \tag{2.11}$$

is used to describe the roll-off factor α in the frequency domain [22].

Figure 2.4a shows possible prototype pulses impulse response, while Figure 2.4b depicts the corresponding power spectral density for each pulse.

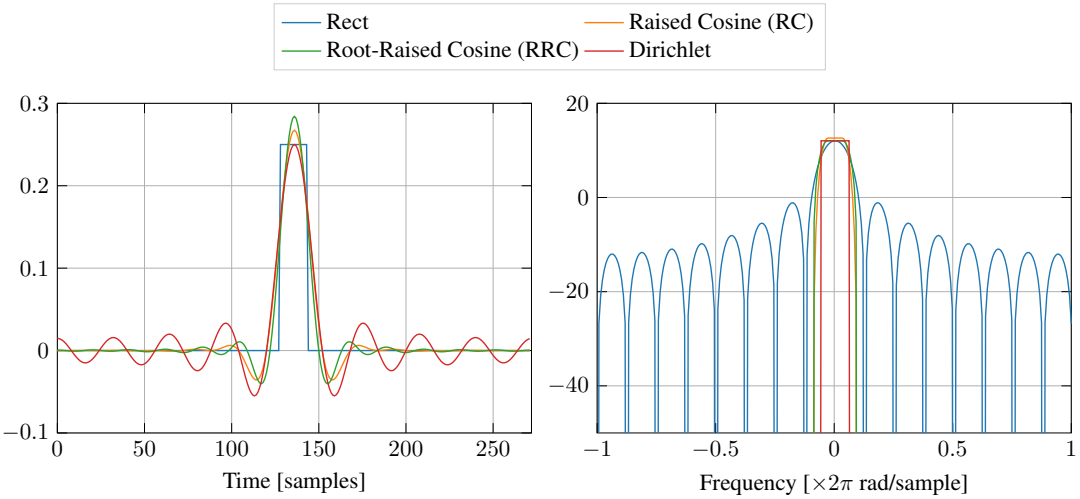

Figure 2.4: *Characteristics of the prototype pulses. a) Filter's impulse response. b) Power spectrum density.*

Table 2.1: *Common GFDM prototype filters.*

Pulse	**Frequency-domain expression**
Raised-Cosine (RC)	$G_{\mathrm{RC}}[f] = \frac{1}{2}\left[1 - \cos\left(\pi \mathrm{lin}_{\alpha}(\frac{f}{M})\right)\right]$
Root Raised-Cosine (RRC)	$G_{\mathrm{RRC}}[f] = \sqrt{G_{\mathrm{RC}}[f]}$
Dirichlet	$G_{\mathrm{Dirichlet}}[f] = G_{\mathrm{RC}}(f)\vert_{\alpha=0}$

The GFDM transmit and receive processing can also be described as matrix operations [21]. The modulated signal vector is given by

$$\mathbf{x} = \mathbf{A}\mathbf{d}, \tag{2.12}$$

where $\mathbf{d}$ is the $(MK \times 1)$ complex-valued data vector and $\mathbf{A}$ is the $(MK \times MK)$ transmit matrix. Its columns are composed by all possible combinations of the K frequency-shifted and the M time-shifted versions of transmitter pulse.

$$\mathbf{A} = \begin{bmatrix} \mathbf{g}_{(0,0)} & \cdots & \mathbf{g}_{(0,K-1)} & \cdots & \mathbf{g}_{(M-1,K-1)} \end{bmatrix}. \tag{2.13}$$

The $(MK \times 1)$ vector $\mathbf{g}_{(m,k)}$ and its N elements are

$$\mathbf{g}_{(m,k)}[n] = g_0[\langle n - mK \rangle_N] \cdot \exp\left(j2\pi \frac{k}{K} n\right). \tag{2.14}$$

Figure 2.5 depicts the a graphical visualization of the transmit matrix. Each column of the transmit matrix represents one time and frequency-shifted version of the prototype

filter kernel. This figure depicts the absolute value of the elements of the GFDM matrix. Each of the elements of the matrix $\mathbf{A}$ is a sample of a shifted version of the prototype filter. The different frequency-shifted versions are shown in groups of K. There are M of such groups, shifted in time. The N rows represent the discrete time instants. The modulation process takes place by weighting each column of the matrix by the data vector. The modulated vector is obtained by performing the summation of the weighted columns.

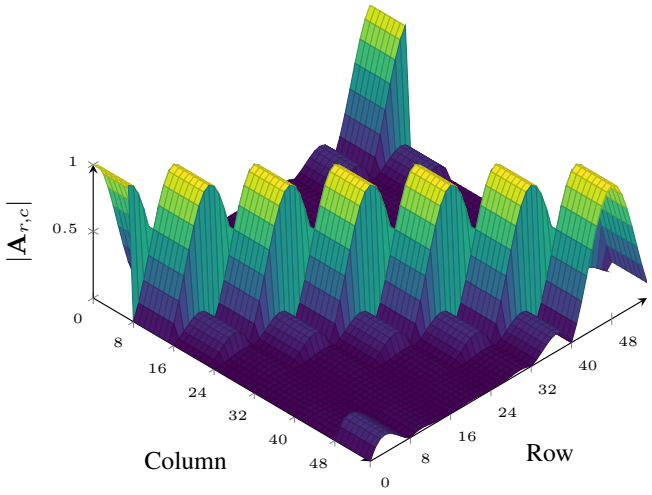

Figure 2.5: *Graphical representation of the GFDM transmit matrix with $M = 7$ subsymbols, $K = 8$ subcarriers using the raised cosine pulse shape filter with $\alpha = 0.5$.*

The GFDM signal is assumed to be transmitted through a time-variant and frequency-selective channel, modeled by its CIR, $\mathrm{h}[n]$. It is assumed that the GFDM symbols is protected by a CP, longer than the CIR duration, and that the channel is constant over the duration of the GFDM symbol. Therefore, the convolution between the $\mathrm{h}[n]$ and the GFDM signal, can be assumed to be circular.

The received signal is given by

$$\mathbf{y} = \mathbf{HAd} + \mathbf{w}, \tag{2.15}$$

where $\mathbf{H}$ is the $MK \times MK$ circulant channel matrix built from $\mathrm{h}[n]$. Also, $\mathbf{w}$ is the additive white gaussian noise (AWGN) vector with zero mean and variance σ_w^2, representing the noise added at the input of the receiver.

The transmitted data is estimated by

$$\hat{\mathbf{d}} = \mathbf{By}, \tag{2.16}$$

where $\mathbf{B}$ is the receive matrix. There are three standard linear receiver matrices, namely ZF, MF, and MMSE.

The MF receive matrix is

$$\mathbf{B}_{\mathrm{MF}} = \mathbf{A}^{\mathrm{H}}. \tag{2.17}$$

The MF receiver results in maximum noise rejection per subcarrier. However, this receive matrix is not able to remove self-interference when non-orthogonal prototype filter is employed on the transmit side [22].

The ZF receive matrix is denoted by

$$\mathbf{B}_{\mathrm{ZF}} = \mathbf{A}^{-1}. \tag{2.18}$$

The ZF receiver is able to fully cancel the self-interference caused by a non-orthogonal transmit matrix. However, it introduces noise amplification which can lead to a SER performance loss.

In both receive techniques stated up to this point, the effect of the selective channel must be treated separately, before the GFDM detection. A ZF equalization is one way to mitigate the effects introduced by the convolution with the CIR leading to [22]

$$\hat{\mathbf{x}} = \underbrace{\mathbf{H}^{-1}\mathbf{H}}_{\text{equalization}}\,\mathbf{A}\mathbf{d} + \underbrace{\mathbf{H}^{-1}\mathbf{w}}_{\text{noise amplification}}. \tag{2.19}$$

By exploiting the circulant property of the channel matrix $\mathbf{H}$, this operation can be inexpensively performed in the frequency-domain, since the channel matrix $\boldsymbol{\mathcal{H}} = \boldsymbol{\mathcal{F}}_N \mathbf{H} \boldsymbol{\mathcal{F}}_N^{\mathbf{H}}$ is diagonal [10]. The components of the main diagonal are the coefficients of the N-point DFT of $\mathrm{h}[n]$. Hence,

$$\mathbf{H}^{-1} = \boldsymbol{\mathcal{F}}_N^{\mathrm{H}} \boldsymbol{\mathcal{H}}^{-1} \boldsymbol{\mathcal{F}}_N. \tag{2.20}$$

This process, however, promotes noise amplification leading to poor SER performance when the channel presents a deep notch in the pass band.

In contrast to ZF or MF, the MMSE receiver jointly performs channel equalization and GFDM detection, minimizing the mean square error between the transmitted and the estimated data symbols, i.e., $\min \mathrm{E}\{\|\mathbf{d} - \hat{\mathbf{d}}\|_2\}$. $\mathrm{E}\{\cdot\}$ is the statistical expectation operator and $\|\cdot\|_2$ is the ℓ^2-norm. The receive matrix for this case is given by [21]

$$\mathbf{B}_{\mathrm{MMSE}} = \left[(\mathbf{H}\mathbf{A})^{\mathrm{H}}(\mathbf{H}\mathbf{A}) + \sigma_w^2 \mathbf{I}_N\right]^{-1} (\mathbf{H}\mathbf{A})^{\mathrm{H}}, \tag{2.21}$$

where $\mathbf{I}_N$ is the $(N \times N)$ identity matrix.

Analyzing the noise variance in (2.21) it is possible to have an intuitive glimpse on how the balance between noise rejection and self-interference cancellation is achieved. As σ_w^2 approaches zero, $\mathbf{B}_{\mathrm{MMSE}}$ approaches the $(\mathbf{H}\mathbf{A})^{-1}$ which is the ZF receiver. When σ_w^2 approaches infinity, in turn, $\mathbf{B}_{\mathrm{MMSE}}$ approaches the MF receiver matrix $(\mathbf{H}\mathbf{A})^{\mathrm{H}}$.

2.4 OFDM and GFDM computational complexity

Modern wireless communication devices use Digital Signal Processing (DSP) to perform the mathematical operations required to transmit and receive radio signals. These calculations can be performed by application-specific hardware, as is the case for Application Specific Integrated Circuit (ASIC), generic hardware like Field-Programmable Gate Array (FPGA), or by a General-Purpose Processor (GPP) in SDR architectures. In any of the previous cases, the number of operations required to transmit or receive signals has a direct impact on cost, silicon area, and energy consumption of the wireless devices.

The complexity of the algorithm required to implement a given technique or waveform plays a vital role in its adoption. It can render a given technology unfeasible for practical implementation on constrained application scenarios, such as mobile phones and Internet of Things (IoT) devices, which may have severe restrictions regarding its size, energy consumption, computational capacity, and cost.

In computer science, the complexity of an algorithm is a measure of the resources needed to perform some computation. The assessment of the complexity of signal processing algorithms usually focuses on two metrics. The number of complex-valued multiplications (CMs), and the big-$\mathcal{O}$ complexity, which describes how the number of required operations scales as the input parameters grow towards infinity as

$$\lim_{N\to\infty} f(N), \tag{2.22}$$

where $f(N)$ is a function that gives the number of operations required for a given algorithm for a input of size N. In the realm of this thesis, N is the amount of the information contained in one block of the waveform.

In linear complexity algorithms, the number of operations scales linearly with the input parameter, while in quadratic algorithms, the number of operations grows with the square of the input parameter. Table 2.2 lists different big-$\mathcal{O}$ complexities.

Table 2.2: *Computational complexity classification in descending order.*

Title	**Complexity**
Factorial	$\mathcal{O}(N!)$
Exponential	$\mathcal{O}(C^N), (C\text{: constant})$
Polynomial	$\mathcal{O}(N^\alpha), (\alpha > 1)$
Quadratic	$\mathcal{O}(N^2)$
Log-linear	$\mathcal{O}(N \log N)$
Linear	$\mathcal{O}(N)$
Logarithmic	$\mathcal{O}(\log N)$
Constant	$\mathcal{O}(1)$

2.4.1 OFDM transceiver Complexity

The implementation of the OFDM waveform is accomplished efficiently by the use of the Fast Fourier Transform (FFT). The K-point FFT takes $(K/2)\log_2 K$ CMs to be computed when the Cooley-Tukey algorithm [23] is employed.

The overall OFDM modulation and demodulation processes can be computed using one Inverse Fast Fourier Transform (IFFT) at the transmitter and one FFT at the receiver, resulting in

$$\mathcal{C}_{\text{OFDM}} = K \log_2 K \text{ CMs}. \tag{2.23}$$

The channel inversion and single-tap equalization processes adds $2K$ multiplications, two per subcarrier, leading to the total amount of $K \log_2 K + 2K$ CMs. The complexity for the OFDM transceiver chain in big-$\mathcal{O}$ notation is $\mathcal{O}(K \log K)$.

2.4.2 ZF GFDM transceiver chain complexity

The GFDM transmitter computes the product of the $(N \times N)$ matrix $\mathbf{A}$ by the $(N \times 1)$ data vector $\mathbf{d}$ which takes N^2 complex-valued multiplications. At the receiver, two processes are performed, the channel equalization and the GFDM detection.

The equalization requires the inversion of the $(N \times N)$ channel matrix $\mathbf{H}$. When computed in frequency domain, it takes only N CMs since the $\boldsymbol{\mathcal{H}}$ is diagonal. However, in this case, the received signal vector $\mathbf{y}$ must be transformed to the frequency-domain for the equalization, and transformed back to the time-domain prior to the GFDM detection. This pair of transforms adds $N \log_2 N$ CMs. The product between the channel inverse and the signal, in the frequency domain, takes N CMs.

Finally the GFDM detection obtained by the product between the equalized signal vector and the receive matrix, takes N^2 CMs, assuming the matrix $\mathbf{A^{-1}}$ is stored pre-computed. The overall number of CMs is then

$$\mathcal{C}_{\text{ZF}} = 2N^2 + N \log_2 N + 2N. \tag{2.24}$$

The complexity of the ZF transceiver chain is $\mathcal{O}(N^2)$.

2.4.3 MF GFDM transceiver chain complexity

The GFDM transmitter computes the product of the $(N \times N)$ matrix $\mathbf{A}$ by the $(N \times 1)$ data vector, which takes N^2 complex-valued multiplications.

At MF the receiver two processes also takes place, the equalization and the GFDM detection. The signal is converted to the frequency-domain and equalized multiplying it by the complex-conjugate of the frequency response. After that, the signal is converted back to the time-domain. The equalization process takes $N \log_2 N + 2N$ CMs, while the GFDM detection takes N^2. The overall GFDM MF transceiver chain requires

$$\mathcal{C}_{\text{MF}} = 2N^2 + N \log_2 N + N \text{ CMs}. \tag{2.25}$$

The complexity of the MF transceiver chain is also $\mathcal{O}(N^2)$.

2.4.4 GFDM MMSE transceiver chain complexity

The GFDM transmitter computes the product of the $(N \times N)$ matrix $\mathbf{A}$ by the $(N \times 1)$ data vector. It takes N^2 operations to compute $x[n]$. In the MMSE receiver, as denoted in (2.21), the detection and channel equalization is jointly performed.

The product $(\mathbf{HA})$ demands N^3 multiplications, since both matrices are $(N \times N)$. The product $(\mathbf{HA})^{\text{H}}(\mathbf{HA})$ results in a symmetric matrix and thus, only $N(N+1)/2$ CMs are required. The operations required to compute the product of the noise variance by the identity matrix $(\sigma^2 \mathbf{I}_{\text{N}})$ can be safely neglected, since this operation is just the repetition of a real-valued scalar.

The inversion of the matrix $[(\mathbf{HA})^{\text{H}}(\mathbf{HA}) + \sigma^{\mathbf{2}}\mathbf{I}_{\mathbf{N}}]$ requires N^3 CMs. The product of the received signal vector by $(\mathbf{HA})$ requires N^2 CMs, and this resulting vector multiplied by the inverse matrix adds N^2 CMs.

The total number of CMs for the MMSE transceiver chain is then

$$\mathcal{C}_{\text{MMSE}} = 2N^3 + \frac{7}{2}N^2 + \frac{1}{2}N, \tag{2.26}$$

resulting in a big-$\mathcal{O}$ complexity of $\mathcal{O}(N^3)$.

A comparison between the OFDM and the classical GFDM transceiver chains is presented in Table 2.3. A more comprehensive comparison is presented in Section 3.2.1.

Table 2.3: *OFDM and Classical GFDM transceiver complexity.*

Technique	**Complex multiplications**	**Complexity**
OFDM	$M \times (K \log_2 K + 2K)$	$\mathcal{O}(N \log N)$
GFDM ZF	$2N^2 + N \log_2 N + 2N$	$\mathcal{O}(N^2)$
GFDM MF	$2N^2 + N \log_2 N + N$	$\mathcal{O}(N^2)$
GFDM MMSE	$2N^3 + 7/2N^2 + N/2$	$\mathcal{O}(N^3)$

2.5 DFT Based GFDM implementation

In the DFT based implementation of the GFDM waveform [24], the GFDM modulation process in (2.10) can be rewritten as

$$x[n] = \sum_{m=0}^{M-1} g_0\left[\langle n - mK \rangle_N\right] \underbrace{\sum_{k=0}^{K-1} d_{k,m} \exp\left(\jmath 2\pi \frac{k}{K} n\right)}_{K\mathscr{F}_K^{-1}\{d_{(\cdot),m}\}|_n}, \tag{2.27}$$

where $\mathscr{F}_K^{-1}\{\cdot\}$ denotes the K-point IDFT of the input data. However, as the discrete-time variable n ranges from 0 to N, the argument of the complex exponential wraps around the unity circle M times. As a result the K-point IDFT is repeated and concatenated M times.

This means that instead of the $N \times MK$ CMs, the inner summation can be calculated once and repeated, reducing the complexity by a factor of M, resulting in $N \times K$ CMs.

This complexity can be further reduced if we consider that the IDFT employed for this calculation uses the FFT algorithm [23]. In this case, the K-point FFT requires only $(1/2)K \log K$ CMs. The number of CMs on the overall modulator process is then $(1/2)MK \log K + MK$. The complexity of the complete transceiver chain, including the equalization, modulator and demodulator for the ZF receiver is

$$\mathcal{C}_{\text{ZF}_{\text{FFT}}} = MK \log_2 K + 2MK + N \log_2 N + 2N \text{ CMs}. \tag{2.28}$$

The authors also extend and apply the same principle to the ZF and MF GFDM demodulator, achieving the same complexity. Unfortunately this principle cannot be directly applied to the MMSE receiver, described by (2.21), since it does not take in account the channel effect.

2.6 Space-time block coding MIMO

MIMO systems are designed to take advantage of the multiple paths existent between the the transmit and receive antennas in order to increase the throughput or increase the robustness of a communication system against fading.

The STBC is based on the Alamouti [25] diversity scheme, which provides a code able to exploit the diversity without decreasing the throughput, relative to the Single-Input/Single-Output (SISO) system. In the Alamouti scheme the data symbols are coded and transmitted over two antennas. The signal undergoes $2J$ different channels to the J receive antennas. Assuming the fading on these channels are uncorrelated, the gain of the resultant channel, after the decoding on the receiver, is equivalent to that of the $2J$ channels added, leading to a diversity of order $2J$.

The Time-reversed Space-Time Block Coding (TR-STBC) [26] is analogous to the Alamouti scheme and was proposed to allow space-time coding for single carrier systems over frequency-selective channels [27]. Although, rather than operating at the complex-valued symbols, it operates at consecutive signal blocks $\vec{x}_i$ and $\vec{x}_{i+1}$. When applied to GFDM, those signal blocks correspond to subsequent GFDM waveform symbols with their respective CP. The signal transmitted at each antenna at two consecutive time intervals is given in Table 2.4

Table 2.4: *TR-STBC signal transmitted at each antenna.*

Time interval	**Antenna 1**	**Antenna 2**
i	$\boldsymbol{\mathcal{F}}^{\mathrm{H}}\vec{X}_i$	$-\boldsymbol{\mathcal{F}}^{\mathrm{H}}\vec{X}^*_{i+1}$
$i+1$	$\boldsymbol{\mathcal{F}}^{\mathrm{H}}\vec{X}_{i+1}$	$\boldsymbol{\mathcal{F}}^{\mathrm{H}}\vec{X}^*_{i}$

In Table 2.4, $\vec{X}$ is the N-point DFT transform of the GFDM waveform signal, $\boldsymbol{\mathcal{F}}$ is the $N \times N$ Fourier matrix and i is an even number. Table 2.4 describes the Alamouti code, however in frequency domain. This code makes the signal transmitted by the antennas orthogonal to each other, consequently enabling discrimination at the receiver.

The TR-STBC diversity scheme is a very attractive technique to be employed in the long range channel due to the increased robustness it can provide. With diversity, even with severe fading occurring between a pair of transmit and receive antennas, a clean reception may still possible due to the channel between another pair of antennas.

The TR-STBC encoding can also be inexpensively obtained using the Fourier transform property

$$\boldsymbol{\mathcal{F}}_N^{\mathrm{H}}\vec{X}^* = x^*[\langle -n \rangle_N], \tag{2.29}$$

then, just the time reversal of the GFDM signal must be obtained. For this reasons this MIMO scheme is included in the performance evaluation of the proposed solution in this thesis.

2.7 Conclusion

Due to the diminishing availability of spectrum, the use of CR in TVWS presents itself as an alternative for broadband connectivity. However, the OOB emissions must be strictly controlled to avoid interference.

The transmission pulse selection in the GFDM waveform allows better control over the spectrum characteristics, resulting in low OOB emissions. GFDM also makes better use of the CP leading to improved spectral efficiency when compared to OFDM. Those characteristics make GFDM an attractive waveform for TVWS and remote area applications.

Modern communications systems use DSP to accomplish the PHY layer processing. Therefore, the complexity of a waveform dictates the cost, silicon area, and energy consumption of wireless devices. The complexity of the classical GFDM ZF and MF receivers is $\mathcal{O}(N^2)$, and can be reduced to $\mathcal{O}(N \log_2 N)$ using the FFT-based implementation. However, the complexity of the GFDM MMSE receiver is $\mathcal{O}(N^3)$ and cannot be reduced with the FFT approach. The complete complexity analysis is presented in Chapter 3.

Another important technique for the long-range scenario is the MIMO for diversity. The TR-STBC can offer improved robustness with low complexity overhead due to the time-reversal property of the Fourier transform.

Chapter 3

Low Complexity Receiver Chain for GFDM

During the work on the laboratory, the development of a GFDM prototype transceiver was needed for field testing. It soon became clear that the MMSE receiver was not feasible due to lack of processing power on the available prototyping platform. However, during the implementation of the Frequency-Domain Equalizer (FDE) for the ZF receiver, another option presented itself. A scheme where a MMSE equalization process would precede the ZF GFDM detection. In this chapter, this proposed receiver chain is presented.

3.1 Proposed Equalization Scheme

The classical linear GFDM MMSE receiver aims at minimizing the Mean Square Error (MSE) between the transmitted complex-valued information symbols, $\mathbf{d}$, and the estimated symbols, $\hat{\mathbf{d}}$, by jointly performing detection and equalization. It offers an adequate balance between white noise rejection and self-interference cancellation. However, the MMSE receive matrix requires matrix inversions in real-time, making its complexity higher than the ZF or MF.

As an alternative, this thesis proposes a simplified receiver chain, where the received signal is equalized prior the GFDM detection using a MMSE FDE. The intent is to reduce the computational complexity associated to the joint process, while offering a better SER performance than the ZF receiver. Instead of estimating the data symbols directly, the estimate of the modulated signal is obtained from the noisy received signal. Only after the equalization process, the GFDM detection is performed to recover the transmitted data symbols. This process is illustrated in Figure 3.1.

The received signal in the frequency-domain can be described as

$$\boldsymbol{\mathcal{F}}_N \mathbf{y} = \mathrm{Y} = \boldsymbol{\mathcal{H}}\mathrm{X} + \mathrm{W}, \tag{3.1}$$

where X is the zero-mean transmitted signal in the frequency-domain, $\boldsymbol{\mathcal{H}}$ is the channel matrix in the frequency-domain, W is the AWGN. Y is the received signal, also in the frequency-domain.

$$\hat{\mathrm{X}} = \boldsymbol{\mathcal{B}}\mathrm{Y}, \tag{3.2}$$

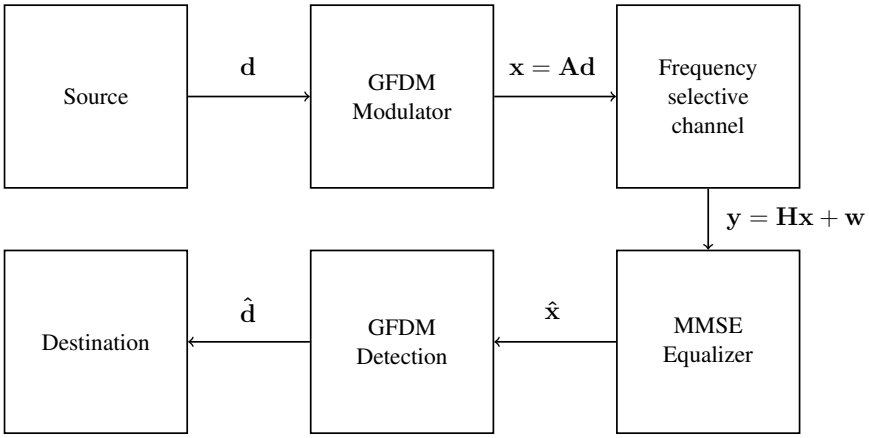

Figure 3.1: *Block diagram for the proposed receive chain.*

is the estimated signal obtained from the noisy received signal. The matrix which minimizes the mean square error between the transmitted signal, X and its estimate, the equalized signal $\hat{\mathrm{X}}$ is

$$\boldsymbol{\mathcal{B}}_{\mathrm{MMSE}} = \arg\min_{\boldsymbol{\mathcal{B}}} \mathrm{E}\{\|\mathrm{X} - \hat{\mathrm{X}}\|_2\}, \tag{3.3}$$

The mean square error (MSE) is given by

$$\begin{aligned} \mathrm{MSE} &= \mathrm{E}\{\underbrace{(\mathrm{X} - \hat{\mathrm{X}})}_{e}\underbrace{(\mathrm{X} - \hat{\mathrm{X}})^{\mathrm{H}}}_{e^{\mathrm{H}}}\} \\ &= \mathrm{E}\{e(\mathrm{X} - \boldsymbol{\mathcal{B}}\mathrm{Y})^{\mathrm{H}}\} = \mathrm{E}\{e\mathrm{X}^{\mathrm{H}} - e(\boldsymbol{\mathcal{B}}\mathrm{Y})^{\mathrm{H}}\} \\ &= \mathrm{E}\{e\mathrm{X}^{\mathrm{H}} - e\mathrm{Y}^{\mathrm{H}}\boldsymbol{\mathcal{B}}^{\mathrm{H}}\} \end{aligned} \tag{3.4}$$

$$\mathrm{MSE} = \mathrm{E}\{e\mathrm{X}^{\mathrm{H}}\} - \underbrace{\mathrm{E}\{e\mathrm{Y}^{\mathrm{H}}\}}_{0}\boldsymbol{\mathcal{B}}^{\mathrm{H}}. \tag{3.5}$$

According to the orthogonality principle for linear estimators, the second term of the MSE is zero for the optimal estimator [28]. The MSE in (3.5) for the MMSE equalizer matrix is

$$\mathrm{E}\{(\mathrm{X} - \boldsymbol{\mathcal{B}}\mathrm{Y})\mathrm{X}^{\mathrm{H}}\} = \mathrm{E}\{\mathrm{X}\mathrm{X}^{\mathrm{H}}\} - \boldsymbol{\mathcal{B}}\mathrm{E}\{\mathrm{Y}\mathrm{X}^{\mathrm{H}}\} \tag{3.6}$$

$\mathrm{E}\{\mathrm{X}\mathrm{X}^{\mathrm{H}}\}$ is the auto-covariance matrix of X, $\mathbf{R}_{\mathrm{XX}}$. $\mathrm{E}\{\mathrm{Y}\mathrm{X}^{\mathrm{H}}\}$ is the cross-covariance matrix between Y and X, $\mathbf{R}_{\mathrm{YX}}$. $\mathrm{E}\{\mathrm{Y}\mathrm{Y}^{\mathrm{H}}\}$ is the auto-covariance matrix of Y, $\mathbf{R}_{\mathrm{YY}}$. Considering that the samples of X are independent with unitary variance, $\mathbf{R}_{\mathrm{XX}} = \mathbf{I}$. The noise auto-covariance matrix is $\mathbf{R}_{\mathrm{WW}} = \sigma_w^2\mathbf{I}$. Hence,

$$\mathbf{R}_{\mathrm{YX}} = \boldsymbol{\mathcal{H}}^{\mathrm{H}}, \tag{3.7}$$

$$\mathbf{R}_{\mathrm{YY}} = \boldsymbol{\mathcal{H}}\boldsymbol{\mathcal{H}}^{\mathrm{H}} + \sigma_w^2\mathbf{I}. \tag{3.8}$$

The MMSE equalizer matrix is then given by

$$\boldsymbol{\mathcal{B}}_{\mathrm{MMSE}} = \boldsymbol{\mathcal{H}}^{\mathrm{H}}(\boldsymbol{\mathcal{H}}\boldsymbol{\mathcal{H}}^{\mathrm{H}} + \sigma_w^2\mathbf{I})^{-1}. \tag{3.9}$$

This expression can be rewritten in the form

$$\boldsymbol{\mathcal{B}}_{\mathrm{MMSE}} = (\boldsymbol{\mathcal{H}}^{\mathrm{H}}\boldsymbol{\mathcal{H}} + \sigma_w^2\mathbf{I})^{-1}\boldsymbol{\mathcal{H}}^{\mathrm{H}}, \tag{3.10}$$

since

$$\begin{aligned}(\boldsymbol{\mathcal{H}}^{\mathrm{H}}\boldsymbol{\mathcal{H}}+\sigma_w^2\mathbf{I})\boldsymbol{\mathcal{H}}^{\mathrm{H}} &= \boldsymbol{\mathcal{H}}^{\mathrm{H}}(\boldsymbol{\mathcal{H}}\boldsymbol{\mathcal{H}}^{\mathrm{H}}+\sigma_w^2\mathbf{I})\\ (\boldsymbol{\mathcal{H}}^{\mathrm{H}}\boldsymbol{\mathcal{H}}\boldsymbol{\mathcal{H}}^{\mathrm{H}}+\sigma_w^2\boldsymbol{\mathcal{H}}^{\mathrm{H}}) &= (\boldsymbol{\mathcal{H}}^{\mathrm{H}}\boldsymbol{\mathcal{H}}\boldsymbol{\mathcal{H}}^{\mathrm{H}}+\sigma_w^2\boldsymbol{\mathcal{H}}^{\mathrm{H}}).\end{aligned} \tag{3.11}$$

The estimated signal is

$$\hat{\mathrm{X}} = \boldsymbol{\mathcal{B}}\mathrm{Y} = \underbrace{(\boldsymbol{\mathcal{H}}^{\mathrm{H}}\boldsymbol{\mathcal{H}}+\sigma_w^2\mathbf{I})^{-1}\boldsymbol{\mathcal{H}}^{\mathrm{H}}}_{\text{MMSE equalization matrix}}\boldsymbol{\mathcal{F}}_N\mathbf{y}, \tag{3.12}$$

which is the optimum estimate of X in the MMSE sense. Equation (3.12) is the well known MMSE equalizer in frequency domain [29].

Using the MMSE FDE, the noise enhancement that would be caused by a zero-forcing equalizer can be avoided. Figure 3.2 depicts the gain of the ZF and MMSE equalizer in a channel with impulse response $h[n] = [1.0, 0.2j, 0.8j]$, and 10 dB signal-to-noise ratio.

From Figure 3.2, it is possible to observe that the ZF equalizer finds the reciprocal of the channel frequency response, introducing very high gains at frequencies severely attenuated by the channel. Hence, the noise at these frequencies are highly amplified (or enhanced), resulting in a performance penalty in terms of SER. The MMSE equalizer, on the other hand, restricts the gain at the severely attenuated frequencies, avoiding the noise enhancement and improving the overall system performance in terms of SER.

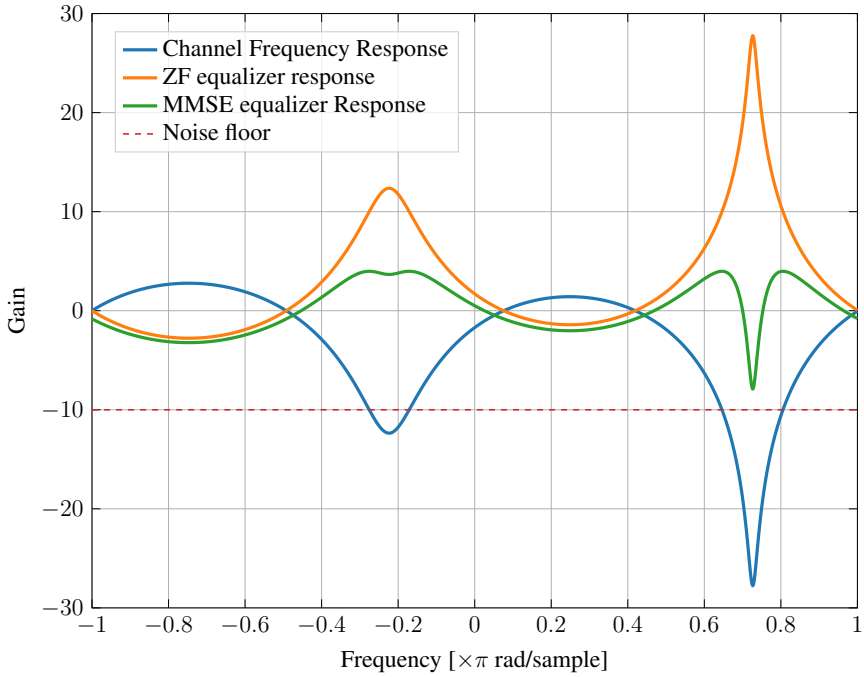

Figure 3.2: *Comparison between ZF and MMSE equalizer frequency response.*

The transmitted data symbols can be recovered from the equalized signal, $\hat{\mathrm{X}}$, by employing the ZF GFDM detection matrix $\mathbf{B}_{\mathrm{ZF}}$. This procedure can introduce a residual noise enhancement because of the behavior of the matrix $\mathbf{B}_{\mathrm{ZF}}$, however this effect is severely reduced when compared with the conventional GFDM ZF receiver.

Figure 3.3 depicts a numerical example of the absolute estimation error with different GFDM receivers. In this example, a GFDM waveform ($K = 64$, $M = 3$ and $\alpha = 0.9$) is transmitted over a frequency-selective channel with the frequency response from Figure 3.2. The absolute error between the transmitted and estimated data symbols, $\mathbf{d}$ and $\hat{\mathbf{d}}$ respectively, is evaluated per subcarrier. The estimation error is

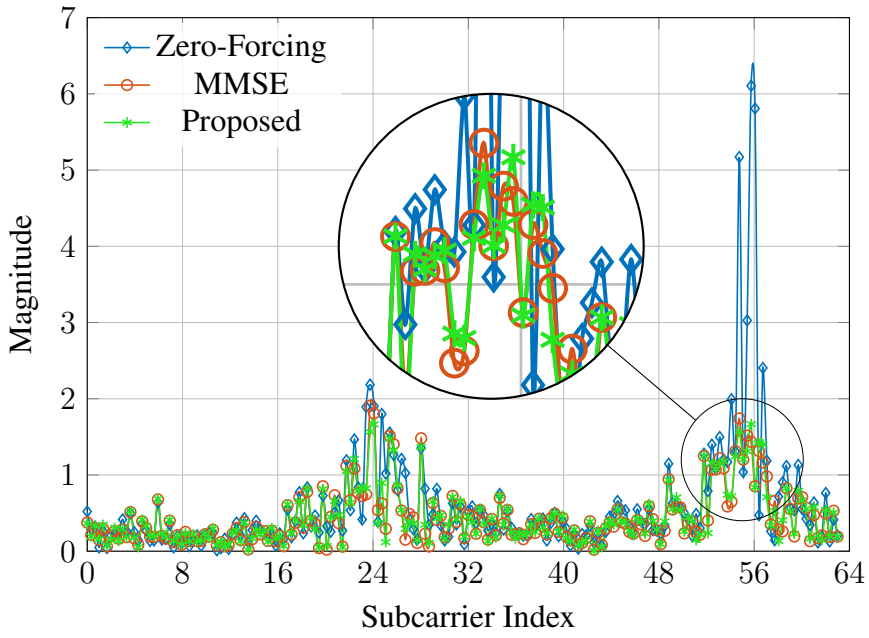

Figure 3.3: *Absolute error for QAM symbols estimated with different receivers, under frequency selective channel.*

accentuated in the most attenuated subcarriers. It is also evident that the ZF receiver produces the highest error in this situation, while the proposed receiver follows closely the MMSE receiver.

The estimated data symbol vector $\hat{\mathbf{d}}$, for the conventional ZF GFDM receiver is

$$\begin{aligned} \hat{\mathbf{d}}_{\mathrm{ZF}} &= \mathbf{A^{-1}H^{-1}HAd} + \mathbf{A^{-1}H^{-1}w} \\ \hat{\mathbf{d}}_{\mathrm{ZF}} &= \mathbf{d} + (\mathbf{A^{-1}H^{-1}})\mathbf{w}. \end{aligned} \tag{3.13}$$

The last term of this equation is the noise vector weighted by the inverse matrix $(\mathbf{HA})^{-1}$. For the proposed scheme, the estimated data vector is

$$\begin{aligned} \hat{\mathbf{d}}_{\mathrm{P}} &= \mathbf{A^{-1}}[(\mathbf{H}^{\mathrm{H}}\mathbf{H}) + \sigma_{\mathbf{w}}^{\mathbf{2}}\mathbf{I}]^{-\mathbf{1}}\mathbf{H}^{\mathrm{H}}\mathbf{HAd} + \mathbf{A^{-1}}[(\mathbf{H}^{\mathrm{H}}\mathbf{H}) + \sigma_{\mathbf{w}}^{\mathbf{2}}\mathbf{I}]^{-\mathbf{1}}\mathbf{H}^{\mathrm{H}}\mathbf{w} \\ \hat{\mathbf{d}}_{\mathrm{P}} &= \frac{(\mathbf{H}^{\mathrm{H}}\mathbf{H})}{(\mathbf{H}^{\mathrm{H}}\mathbf{H}) + \sigma_{\mathbf{w}}^{\mathbf{2}}\mathbf{I}} \cdot \mathbf{d} + \mathbf{A^{-1}}[(\mathbf{H}^{\mathrm{H}}\mathbf{H}) + \sigma^{\mathbf{2}}\mathbf{I}]^{-\mathbf{1}}\mathbf{H}^{\mathrm{H}}\mathbf{w}. \end{aligned} \tag{3.14}$$

In estimation theory, an estimator is said biased if the expected value of the parameter being estimated is different from the actual value. The estimate $\hat{\mathbf{d}}_{\mathrm{ZF}}$ is unbiased since

$$\begin{aligned} \mathrm{E}\{\hat{\mathbf{d}}_{\mathrm{ZF}}\} &= \mathrm{E}\{\mathbf{d}\} + \mathrm{E}\{(\mathbf{A^{-1}H^{-1}})\mathbf{w}\} \\ &= \mathbf{d} + \mathrm{E}\{(\mathbf{A^{-1}H^{-1}})\}\mathrm{E}\{\mathbf{w}\} \\ &= \mathbf{d}, \end{aligned} \tag{3.15}$$

as w is AWGN with zero mean. However, the estimated signal for the proposed scheme, $\hat{\mathrm{X}}$ is biased, since

$$\begin{aligned} \mathrm{E}\{\hat{\mathrm{X}}\} &= \mathrm{E}\left\{[(\boldsymbol{\mathcal{H}}^{\mathrm{H}}\boldsymbol{\mathcal{H}}) + \sigma_w^2\mathbf{I}]^{-1}(\boldsymbol{\mathcal{H}}^{\mathrm{H}}\boldsymbol{\mathcal{H}})\right\} \cdot \mathrm{d} \\ &= \beta\mathrm{X}. \end{aligned} \tag{3.16}$$

The biasing can be removed scaling the estimated signal,

$$\hat{\mathrm{X}}_{\mathrm{unbiased}} = \beta^{-1} \cdot \hat{\mathrm{X}}, \tag{3.17}$$

where β is [30, 31]

$$\beta = \frac{1}{1+\sigma_w^2}. \tag{3.18}$$

In the frequency-domain, the channel matrix $\boldsymbol{\mathcal{H}}$, its Hermitian $\boldsymbol{\mathcal{H}}^{\mathrm{H}}$, and the noise variance matrix $\sigma_w^2\mathbf{I}_N$ from (3.12) are diagonal and, as a result, the inverse of the resulting matrix reduces to the element-wise reciprocal of the main diagonal, decreasing considerably the number of required operations.

It should be noted that in the proposed equalization scheme, the noise variance σ_w^2 needs to be estimated at the receiver. This step is not needed when using the classical ZF equalization. Figure 3.4 shows the block diagram for the proposed receiver chain with the MMSE equalizer described in (3.12). A summary of the complexity required to perform GFDM decoding and equalization is provided in Section 3.2.

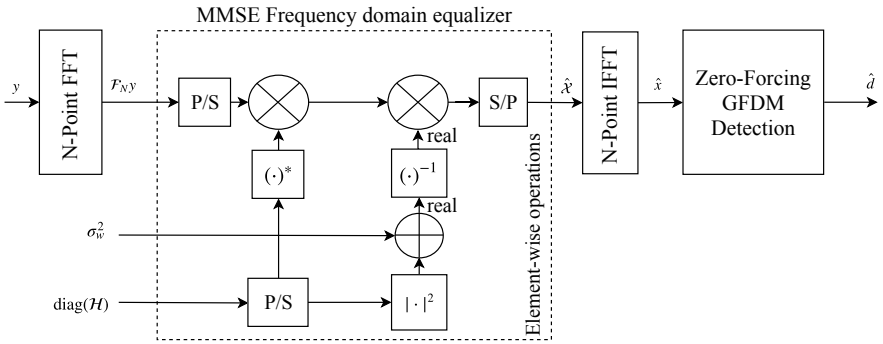

Figure 3.4: *Frequency-domain MMSE Equalizer block diagram.*

Despite other equalization schemes, such as decision feedback equalizer, could also be combined with the GFDM detection process, this thesis concentrated the focus on linear processes.

3.2 Proposed scheme complexity reduction

The proposed receiver chain takes $N \log_2 N$ complex-valued multiplications to compute one DFT/IDFT pair necessary for the FDE. Knowing that $\boldsymbol{\mathcal{H}}$ is diagonal, the product $\boldsymbol{\mathcal{H}}^{\mathrm{H}}\boldsymbol{\mathcal{H}}$ in (3.12) is calculated in N operations. In fact, this product can be calculated alternatively as $|\mathrm{diag}(\boldsymbol{\mathcal{H}})|^2$. This takes two real-valued multiplications per diagonal element, as opposed to four, required in complex multiplication. The matrix inversion, as required in (3.12), adds N complex multiplications, as well as the equalization product.

The GFDM detection employed on the proposed scheme is the ZF, which takes N^2 operations. The overall complexity for the proposed chain, including the transmitter, MMSE FDE channel equalizer and the ZF GFDM detection is given by

$$\mathcal{C}_{\mathrm{P_{ZF}}} = 2N^2 + N\log_2 N + \frac{5}{2}N, \tag{3.19}$$

leading to a complexity of $\mathcal{O}(N^2)$.

3.2.1 Further complexity reduction

For the complexity calculation in the previous sections, the classical linear GFDM detection methods were employed. Although, it is important to notice that in the proposed receiver chain the MMSE FDE channel equalizer can be followed by any linear GFDM detection process. The FFT-based time domain implementation proposed in [24] and, briefly described in section 2.5, can be employed to further reduce the complexity of the GFDM detection, while keeping the improved performance.

With this implementation, the GFDM detection takes M DFTs of size K, followed by MK multiplications. The transmitter requires the same amount of CMs.

In this case, the overall complexity for the proposed transceiver is

$$\mathcal{C}_{\mathrm{P_{FFT}}} = MK\log_2 K + 2MK + N\log_2 N + \frac{5}{2}N \text{ CMs}. \tag{3.20}$$

Table 3.1 presents a summary of the complexity of the receivers. Figure 3.5 depicts

Table 3.1: *GFDM and OFDM transceiver complexity*

Technique	Complex multiplications	Complexity
GFDM MMSE	$2N^3 + 7/2N^2 + N/2$	$\mathcal{O}(N^3)$
GFDM ZF	$2N^2 + N\log_2 N + 2N$	$\mathcal{O}(N^2)$
GFDM MF	$2N^2 + N\log_2 N + N$	$\mathcal{O}(N^2)$
GFDM Proposed (ZF)	$2N^2 + N\log_2 N + 5N/2$	$\mathcal{O}(N^2)$
GFDM ZF-FFT [24]	$(MK)\log_2 K + 2MK$ $+N\log_2 N + 2N$	$\mathcal{O}(N\log N)$
GFDM Proposed (FFT)	$MK\log_2 K + 2MK$ $+N\log_2 N + 5N/2$	$\mathcal{O}(N\log N)$
OFDM	$M \times (K\log_2 K + 2K)$	$\mathcal{O}(N\log N)$

how the number of CMs increases with the number of subcarriers K for a constant M.

The values of K used in this graph are consistent with the number of subcarriers used in communications current wireless communications systems systems such as the IEEE 802.11, Integrated Services Digital Broadcasting (ISDB-T) or Digital Video Broadcasting version 2 (DVB-T2) that have a number of subcarriers between 64 and 31072.

The graphic depicts the number of CMs in a logarithmic scale to accommodate the large variation in the complexity. In Figure 3.5, it is possible to clearly identify three distinct groups, matching the Big-$\mathcal{O}$ complexities of $\mathcal{O}(N \log N)$, $\mathcal{O}(N^2)$ and $\mathcal{O}(N^3)$. In practice, the number of operations in the order of 10^{13}, for the cubic complexity group, means that this receivers are not feasible for practical systems.

For completeness, in Figure 3.6, K is kept constant while M is increased. Despite the slightly increased complexity of the GFDM implementations in comparison with Figure 3.5, the overall asymptotic behavior is the same.

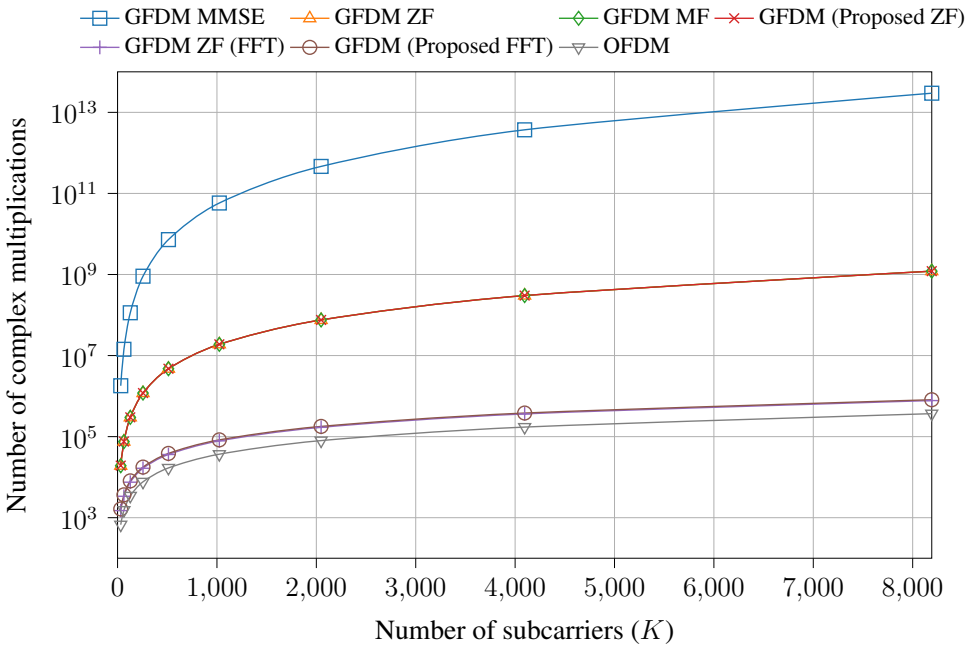

Figure 3.5: *Numerical evaluation of the number of complex-valued multiplications versus number of subcarriers K for ($M = 3$).*

3.3 SER Performance evaluation

The SER performance of the proposed scheme was simulated considering a time-variant multi-path channel. First, a SISO scheme was assumed. Diversity gain from a 2-by-2 MIMO based on time-reversal STBC has also been analyzed, assuming that the channel coherence time is higher than two GFDM block length.

For practical reasons, a bandwidth of 240 kHz, analogous to a Resource Block (RB) on a LTE system, is simulated. The simulation assumes propagation in the UHF band for long-range applications. The maximum channel delay spread is assumed to be 66.66μs and it is in agreement with the literature [32].

The channel impulse response used to model the time-variant FSC has 16 taps composed by complex Gaussian random variables with zero mean and unitary variance, weighted by a power delay profile, linearly decaying from 0 to -10 dB.

The FSC fading is implemented in a block fashion. While this assures that the channel is constant withing a block, it allows for statistically independent CIRs in

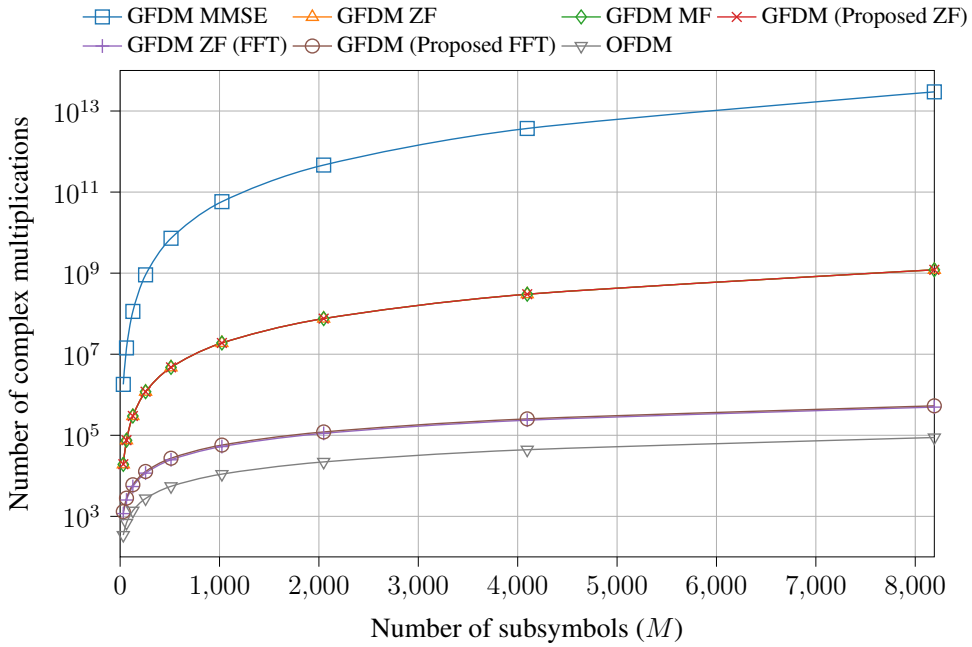

Figure 3.6: *Numerical evaluation of the number of complex-valued multiplications versus number of subsymbols M for ($K = 3$).*

subsequent blocks. A Monte Carlo simulation was implemented in MATLAB using the GFDM library, made available by the Vodafone Chair for Mobile communication Systems of the Technische Universität Dresden [33].

The parameters used in the simulations are shown in Table 3.2. Perfect synchronization and knowledge of the Channel State Information (CSI) is assumed.

Table 3.2: *SER simulation parameters*

Parameter	**Value**
Prototype filter	Raised Cosine
Roll-off factor (α)	0.9
Constellation Mapping	16 QAM
Number of subsymbols (M)	3
Number of subcarriers (K)	64 (240 kHz)
Cyclic-Prefix size (N_{cp})	16 samples (66.66μs)
Sample frequency	240 kHz
Subcarrier spacing	3.75 kHz
Channel excess delay	16 samples (66.66μs)

The SER performance under time-variant FSC is depicted in Figure 3.7. As opposed to what occurs in the AWGN channel, the equalizer needs to compensate for the non-flat frequency response of the channel and, as pointed in Section 2.3, noise enhancement occurs when using ZF equalization. The MMSE receiver and the proposed receiver have the same SER performance in this situation, over-performing the ZF receiver.

The performance gain of the proposed scheme, over the ZF, increases with signal-to-noise ratio approaching asymptotically the the gain of the MMSE over the ZF. The modest value of 0.25 dB reflects the low probability of deep fading in the channel frequency response for the channel used in the simulation. This value, however, can be higher depending on the channel model and its practical significance depends largely on the application.

In Figure 3.8, the SER performance of the proposed equalizer is shown assuming a 2-by-1 STBC scheme over time-variant FSC. The correlation between the impulse response of both paths from the two transmit antennas to the receive antenna is given by the parameter ρ, where a value equals to 1 means that the impulse response of the paths are identical. In STBC, the equivalent channel response of the MIMO channel can be described by $\boldsymbol{\mathcal{H}}_{\text{eq}} = |\boldsymbol{\mathcal{H}}_{11}|^2 + |\boldsymbol{\mathcal{H}}_{21}|^2$, where $\boldsymbol{\mathcal{H}}_{ij}$ is the frequency response of the channel between the i-th transmit antenna and the j-th receive antenna. In this way, it is unlike that both channels have a high attenuation on the same frequency, unless they are strongly correlated. As a consequence, the proposed scheme just shows improvement over the ZF equalizer in the event of correlated channels.

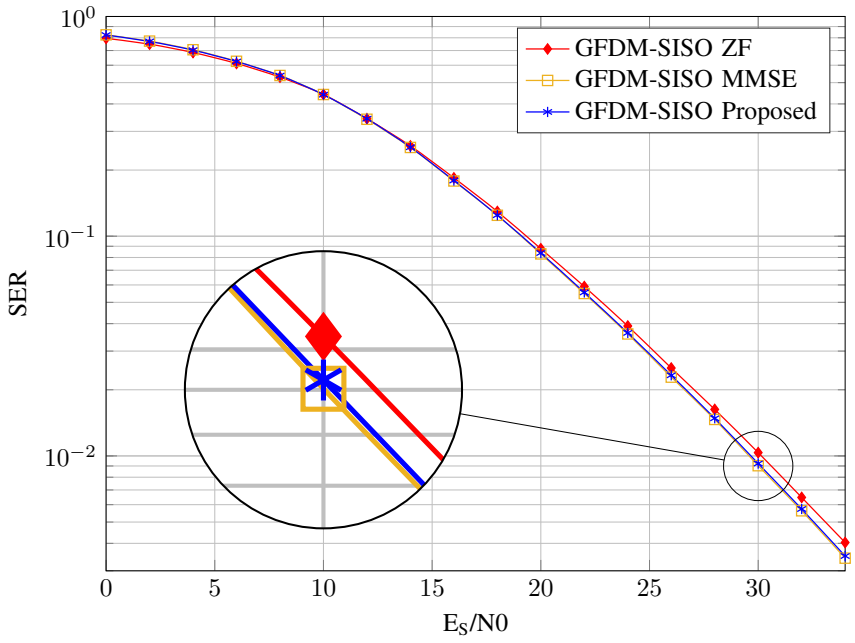

Figure 3.7: *Comparison between the symbol error rate of the proposed scheme under time-variant FSC channel with a roll-off* $\alpha = 0.9$.

3.4 Conclusion

The GFDM MMSE receiver has better performance than the ZF and MF. It jointly equalizes the channel and performs the GFDM detection providing a balance between self-interference cancellation and noise rejection. However, it is computationally expensive and this fact can prevent its employment in some practical applications.

This thesis proposes a simplified receiver chain where the channel effects are addressed using a FDE MMSE equalizer. Subsequently, the GFDM detection is per-

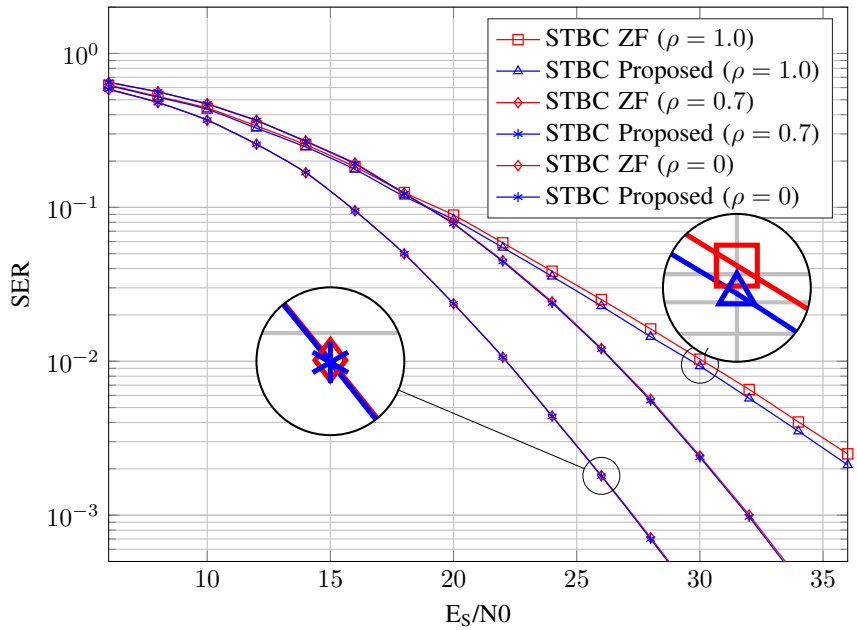

Figure 3.8: *Comparison between the symbol error rate of the proposed scheme assuming 2-by-1 STBC and time-variant FSC channel with a roll-off $\alpha = 0.9$ for various values of correlation between the channels.*

formed by ZF receiver. The proposed chain avoids the noise enhancement caused by the ZF due to de channel frequency response.

The proposed receiver chain offers a complexity of $\mathcal{O}(N^2)$, that can be further reduced to $\mathcal{O}(N \log_2 N)$ using the FFT-based GFDM detection.

Simulations show SER performance improvement in comparison to ZF. This improvement is noticeable in the SISO channel where a deep fading, in frequency response, is more likely than in the TR-STBC MIMO equivalent channel.

Chapter 4

Software Defined Radio Implementation

The previous chapters evaluate the proposed receiver chain using theoretical evaluation and numerical simulation. However, the feasibility of the given scheme in real communications systems is also dependent on the capability of the currently available hardware.

Chapter 4 has the primary goal of evaluating the proposed receiver regarding its applicability to real-life communications systems. To this end, the proposed transceiver was implemented in a Software Defined Radio prototype. The techniques necessary to achieve an implementation capable of harvesting the full potential of modern processors are presented.

While the content of this chapter differs significantly from the previous, it also aims to narrow the gap between the theoretical evaluation and practical implementation.

4.1 Software Define Radio

SDR is a set of DSP functions combined to integrate a transceiver, performing real-time communications while hosted in a GPP. In this approach, most of the signal processing is done by a non-specialized processor, such as x86-64 and ARM, found in personal computers and embedded platforms.

SDR based equipment can be produced at a lower cost than equipment based on dedicated hardware, since commercial off-the-shelf components, produced in high volumes, can be used for the signal processing [34]. Affordable equipment can reduce the entry barrier for small network operators and Internet Service Providers (ISPs) to deploy access networks in areas that are not attractive to classical mobile operators. Besides that fact, SDR implementation of communications systems are highly flexible, since communication techniques can be modified at run-time by software updates.

FPGAs can achieve high efficiency and high computation power using the parallel processing and, at first glance, could be seen as a better solution for PHY development when compared with GPPs. However, modern multi-core GPPs operates at higher clock frequencies and implements several techniques to fully exploit the silicon fea-

tures, such as Single Instruction Multiple Data (SIMD), instruction pipeline and out-of-order speculative execution. These modern processors can achieve a computational power higher than a FPGA. Although, to fully exploit the potential of such processors, the code must take advantage of all features offered by the GPP.

While modern compilers are able identify parallelism in software loops, the use of explicit vectorization using machine code can, in the other hand, guarantee the execution of parallel operations.

4.2 GFDM waveform in C/C++ language

During the course of the studies related to this thesis, a real-time GFDM modem using the SDR approach was implemented. The implementation is based on the algorithm using the FFT, as described in Section 2.3, once this approach leads to a low complexity implementation, suitable for real-time application in SDR.

The low complexity algorithm for the GFDM modulator takes the array of complex data symbols to be to be modulated and executes M IFFTs of size K. The elements of the resultant vector are multiplied by the transmission pulse, which is pre-calculated and stored in memory. The vector with the transmission pulse is circularly-shifted by K samples and the element-wise multiplication is repeated. This process is repeated M-times and the results of each iteration are accumulated. The FFT-based GFDM modulation process is depicted in Figure 4.1. At the demodulator, the process is al-

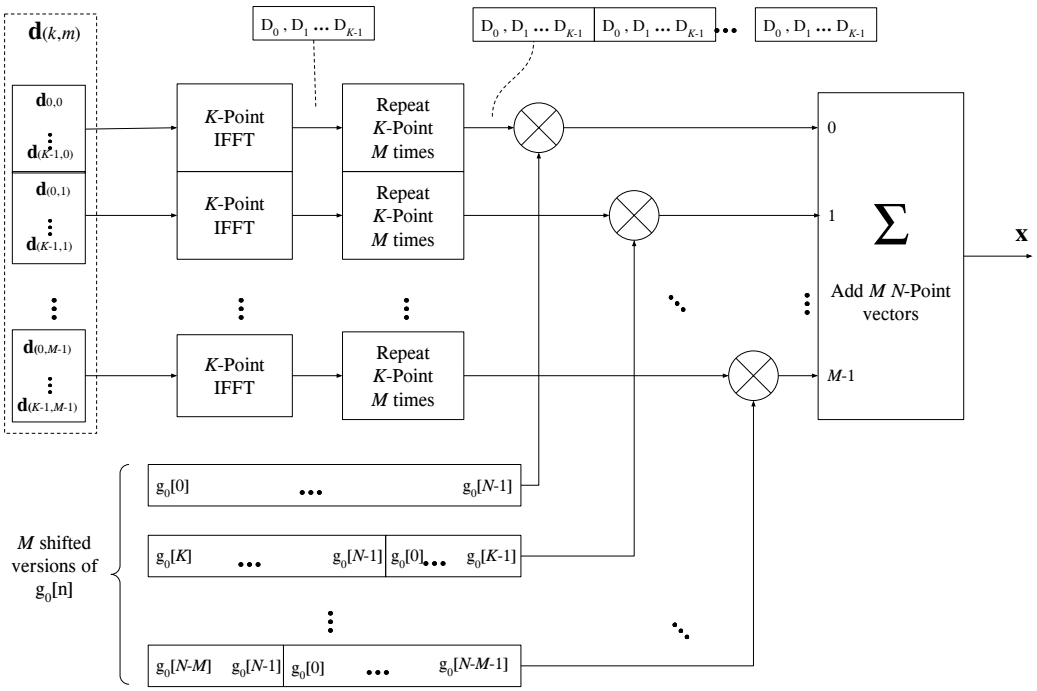

Figure 4.1: *FFT-based GFDM modulator block diagram.*

most the same. However, the order of the operations and the direction of the shift are reversed. The IFFTs operations are also replaced by M IFFTs of size K. The last difference is the pulse shape, which is replaced by the receiver pulse, which is also

pre-calculated and stored in memory. This process is depicted in Figure 4.2.

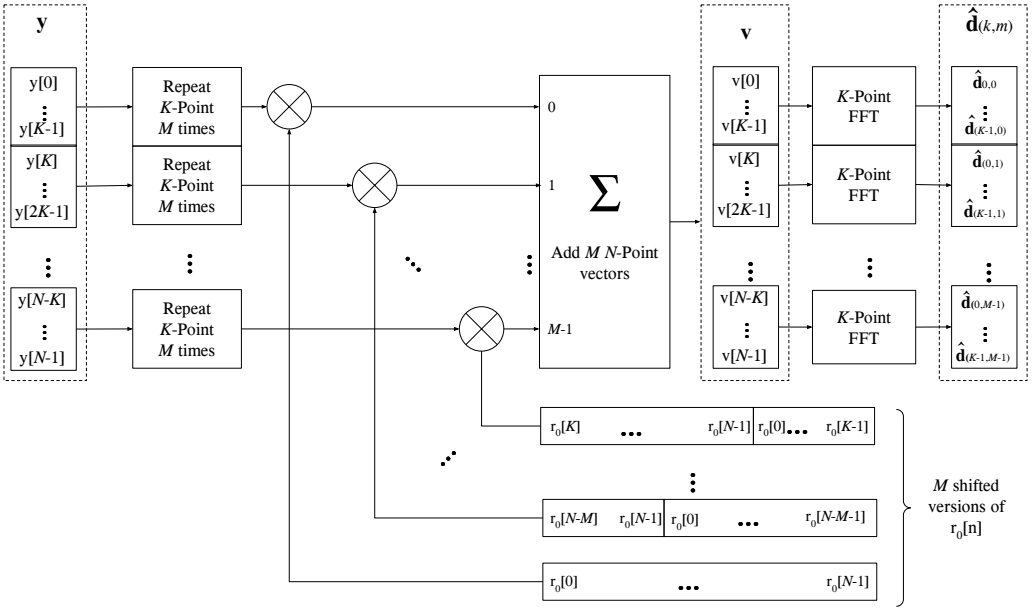

Figure 4.2: *FFT-based GFDM demodulator block diagram.*

At the receiver side, the signal is equalized with the frequency domain MMSE equalizer, described in Section 3.1. The implementation of the equalizer uses a pair of $N-$point FFT and IFFT.

The FFT implementation uses the Fastest Fourier Transformer in the West (FFTW) library [35], which is a open-source and high performance implementation of Cooley-Tukey DFT algorithm and other variants. This library is able to offer high performance in computing DFTs, where the size N can be decomposed in small primes in the form

$$N = 2^P + 3^Q + 5^R + 7^S. \tag{4.1}$$

Despite the fact that the maximum performance can be obtained for S being a power of two, the possibility to use primes up to 7 makes it attractive for the GFDM implementation with an odd number of sub-symbols or sub-carriers. This library conveniently offers functions optimized for the execution of multiples transforms of the same size, as required by the GFDM waveform implementation. Another important aspect of the FFTW is that it uses SIMD instructions, making efficient use of modern GPP.

The SDR implementation of the GFDM waveform was written in C and C++ and compiled using the open-source GNU C Compiler (GCC) [36] targeting the x86-64 architecture, more specifically, the 8-Core INTEL Core-i9 9900K processor which, in turn, features the INTEL Advanced Vector Extensions 2 (AVX2) instruction set.

As many modern compilers, GCC is able to perform auto-vectorization of loops, identifying operations that are independent and can be carried-out as vector operations at the SIMD unit of the processor. Unfortunately, the compiler is not able identify all vectorization opportunities automatically and other techniques can be used to direct the compiler, such as Open Multi-Processing (OpenMP) or, in a more explicit way, using intrinsics [37].

OpenMP makes possible to use directives to guide the compilation process. With OpenMP, the programmer can provide explicit information about data dependency and other issues, such as pointer aliasing, that may prevent the compiler auto-vectorization. With the addition of few directives at critical sections of the code, it is possible to obtain the desired vectorization. The listing below shows portion of the GFDM modulator code where a OpenMP directive is employed to achieve vectorization.

```
#pragma omp simd aligned(input, output, pulse : 32)
for (int k = 0; k < K; k++)
{
    output[k] += (input[k] * pulse[k]);
}
```

Program 4.1: *OpenMP directed vectorization of a **for** loop*

Intrinsics, on the other hand, are high level language functions that maps almost directly to low-level machine instructions. While they offer high control over the instructions generated by the compiler, it makes the source code tightly coupled to the underlying hardware, reducing the flexibility and portability of SDR. Intrinsics were used in small critical portions of the modulation process in the inner-most part of nested loops. As those sections are executed a large number of times, any performance loss is relevant. The code below implements the same loop depicted in Program 4.2 but using intrinsics, for comparison purposes. In this loop a complex-valued float number multiplication is implemented using AVX2 intrinsics and is able to carry four complex-valued float numbers at every loop iteration.

```
for (int k=0; k < K; k += 4)
{
    __m256 r1, r2, r3;
    __m256 vecIn    = _mm256_load_ps((float*) input);
    __m256 vecOut   = _mm256_load_ps((float*) pulse);
    __m256 vecPulse = _mm256_load_ps((float*) output);

    // AVX length 4 Complex multiplier
    r1 = _mm256_addsub_ps(-_mm256_mul_ps(vecIn, vePulse));
    r2 = _mm256_mul_ps(vecIn,_mm256_permute_ps(vecPulse, 0xB1));
    r3 = _mm256_permute_ps(_mm256_hadd_ps(r1, r2), 0xD8);
    vecOut = _mm256_add_ps(r3, vecOut);
    _mm256_store_ps(((float*) output), vecOut);
}
```

Program 4.2: ***for** loop using AVX2 INTEL intrinsics*

4.3 Implementation results and details

The software GFDM transceiver, with the proposed equalizer, was compiled using the principles and techniques presented in Section 4.2. The resulting software was executed as real-time demonstrations. The processing performance was measured with the Google benchmark library [38]. With this approach, it is possible to predict the real-time performance. The SDR implementation was tested under different waveform parameters and, the achieved sample rate, is an indicative of the radio-frequency

bandwidth attainable by the implementation. The results are summarized in Table 4.1, where it can be seen that a bandwidth up to 498 MHz can be processed using the test computer. However the real system performance depends on other factors, such as the

Table 4.1: *SDR implementation performance for various waveform parameters*

K	M	**Time per symbol [ns]**	**Sample Rate [Ms/s]**
1024	2	4105	498.8
1536	2	7110	432.0
3072	2	17392	353.2
8192	2	48161	340.1
65536	2	1717895	76.30
1024	3	7311	420.2
3072	3	26353	349.7
8192	3	103491	237.4
65536	3	1289530	152.4
1024	4	10090	405.9
3072	4	39867	308.2
8192	4	122352	267.8
65536	4	2474764	105.9

Central Processing Unit (CPU) usage by other tasks, related or not with the communication system signal processing chain. Another important consideration for a practical system is the bandwidth available to transfer the samples between the host computer and the radio interface. The SDR implementation was connected to a radio platform able to deliver 160 MHz of bandwidth. Figure 4.3 shows a picture of the Intel i9 host computer and the National Instruments USRP 2974R SDR platform used for the testbed. Table 4.2 describes the characteristics of the equipment and the parameters used in the implementation. The spectrum of the signal generated by this platform is

Table 4.2: *SDR transceiver hardware and software characteristics.*

Hardware/Software element	**Characteristics**
Host Computer	Intel Core i9-9900K (8 cores) 16 GB of RAM
SDR platform	National Instruments USRP 2954R
Software Implementation	C and C++
System sample rate	200 Msps
Maximun Radio Bandwidth	160 MHz
Programming techniques and libraries	FFTW, AVX2 Intrinsic, OpenMP

depicted in Figure 4.4. This picture was taken from the screen of an Agilent E4403B

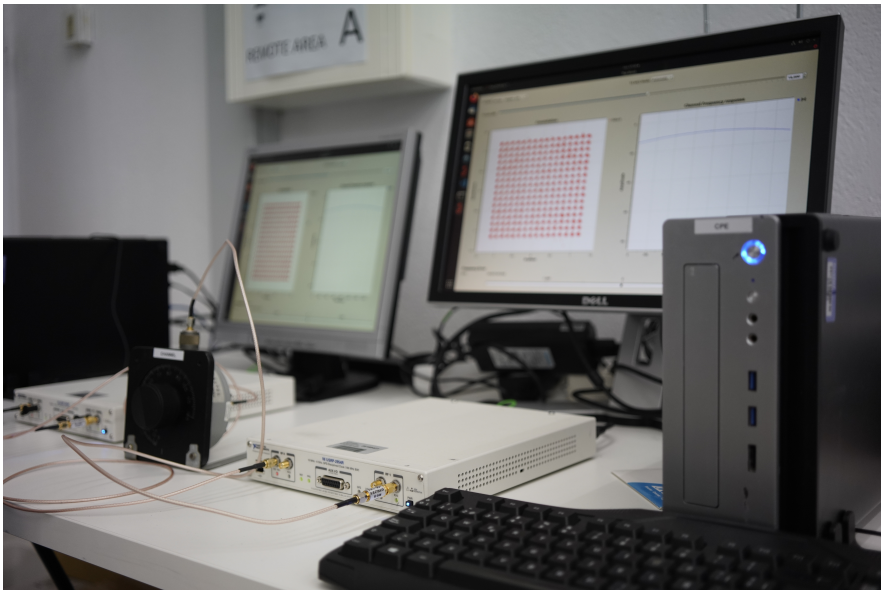

Figure 4.3: *Host computer and hardware SDR platform.*

spectrum analyzer where the signal bandwidth were measured. The SDR implementation was capable of delivering 100 Msps, consistent with the performance predicted in Table 4.1. This results in a RF bandwidth of 84 MHz, limited by the interpolation and reconstruction filters of the transceiver. Such a result proves that this implementation capable of being employed in real-time communication system.

Later, this implementation was integrated to the physical layer of the 5G-Range proof-of-concept prototype transceiver [34].

4.4 Conclusion

SDR employs GPPs to perform real-time DSP. Due to the mass production of those commercial-off-the-shelf platforms, the SDR approach enables affordable radio transceivers, reducing the overall cost to deploy wireless networks in remote areas.

Modern GPPs can deliver high computational power. However, to achieve real-time DSP performance, the fine-grained parallelism provided by the SIMD units of the processor must be exploited. This can be achieved explicitly using SIMD intrinsics, or indirectly, by guiding the compiler using OpenMP.

The FFT-based GFDM modulator and demodulator were implemented in C and C++ language, targeting the x86-64 architecture. Critical sections of the software were implemented using Intel AVX2 intrinsics and OpenMP directives while the required FFT/IFFT transforms were realized using the well-known open-source FFTW library.

The obtained software was tested in an Intel i9-9900K using the Google benchmark library. The results suggest that sample rates as high as 498 MS/s would be achievable. However, other factors, such as concurrent tasks and baseband data transfer to the radio platform, limit the real-life performance. The host computer, running the SDR implementation, was connected to a radio transceiver and sustained a sample rate of 100 Msps with a signal bandwidth of 84 MHz. Later, this software was used in the

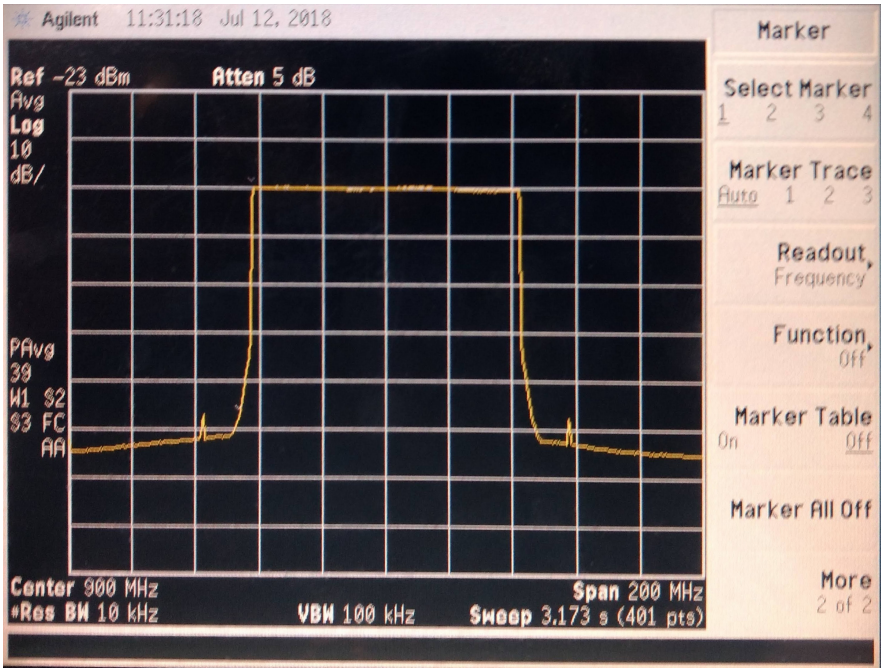

Figure 4.4: *Spectrum of the GFDM signal with* $K = 65536$*,* $M = 4$*, and* 84 *MHz bandwidth.*

5G-Range proof-of-concept prototype. The results suggest that the proposed GFDM chain can be used in practical communication system.

Chapter 5

Conclusion and Final Considerations

This thesis proposed a new scheme of equalization for the GFDM waveform where, the channel is equalized in the MMSE sense in the frequency domain. In this scheme, the noise enhancement caused by the equalization of the channel frequency response can be avoided. However, the noise enhancement caused by the GFDM detection process is not addressed, therefore, not mitigated.

The proposed scheme is not optimal in the MSE sense of the data symbols $\mathbf{d}$, but it offers a complexity of $\mathcal{O}(N^2)$, which is the same of the ZF GFDM, while the complexity of the MMSE GFDM is $\mathcal{O}(N^3)$. Although, the exact number of CMs is still slightly larger than the ZF.

The proposed receiver chain can also employ the implementation of the GFDM detection based on FFT, resulting in a complexity of $\mathcal{O}(N \log_2 N)$, which is, in turn, the same complexity observed by the OFDM waveform, making its implementation affordable in practical real-time communication systems. Again, the exact number of CMs is still slightly higher than in the OFDM waveform.

The proposed scheme is fairly generic and the equalizer-detector cascade can be used in other orthogonal and non-orthogonal waveforms described in matrix notation, i.e. Orthogonal time frequency space (OTFS) modulation [39], providing complexity gain over the direct matrix inversion implementation of the MMSE.

The simulation shows that the proposed scheme improves the SER performance, when compared to the ZF receiver under SISO and STBC MIMO frequency selective channels. It also shows that the SER improvement is more noticeable in SISO channel, where deep fadings in the overall frequency response are more likely to occur. For future work, the closed form expression for the SER performance of the proposed scheme can be derived, allowing to better quantify the benefit of using such scheme.

The GFDM transceiver was implemented using a SDR approach in C/C++ language, targeting the x86-64 architecture. It employs the FFT-based GFDM detection using the FFTW library. OpenMP and AVX2 vectorization techniques are used to effectively exploit the SIMD units available at modern processors, unlocking its potential for real-time applications.

A benchmark executed using the Google benchmark library shows that the attainable sample rate for this implementation are compatible with real-time performance

when running in a Intel i9-9900K processor. Finally, the implementation was tested in a SDR platform, in real-time, generating a 84 MHz wide signal, showing that this approach is suitable for practical applications.

Chapter 6

Published papers

This Chapter presents the list of papers published by the author during the development of the research presented in this master's thesis.

6.1 Papers published as author

W. Dias, L. Mendes and J. Rodrigues, *"Low Complexity GFDM Receiver for Frequency-Selective Channels,"* in *IEEE Communications Letters*, vol. 23, no. 7, pp. 1166-1169, July 2019.

W. Dias, A. Ferreira, R. Kagami, J. Ferreira, D. Silva and L. Mendes, "5G-RANGE A transceiver for remote areas based on software-defined radio," *2020 European Conference on Networks and Communications (EuCNC)*, 2020, pp. 100-104.

W. Dias et al., "Performance Analysis of a 5G Transceiver Implementation for Remote Areas Scenarios," *2018 European Conference on Networks and Communications (EuCNC)*, 2018, pp. 363-367.

W. Dias, M. Carleti, S. Moreira and L. Mendes, "Evaluation of Rain Attenuation Models in Satellite Links under Tropical and Equatorial Climates," in *IEEE Latin America Transactions*, vol. 16, no. 2, pp. 358-367, Feb. 2018.

6.2 Papers published as co-author

A. Ferreira, W. Dias, et al.,"5G-RANGE Project Field Trial," *2019 European Conference on Networks and Communications (EuCNC)*, 2019, pp. 490-494.

L. Mendes, et al., "Enhanced Remote Areas Communications: The Missing Scenario for 5G and Beyond 5G Networks," in IEEE Access, vol. 8, pp. 219859-219880, 2020.

Bibliography

[1] L. J. Vora, "Evolution of mobile generation technology: 1G to 5G and review of upcoming wireless technology 5G," *Int. J. of Modern Trends in Engineer. and Research*, vol. 2, no. 10, pp. 281–290, 2015.

[2] L. L. Mendes, C. S. Moreno, M. V. Marquezini, A. M. Cavalcante, P. Neuhaus, J. Seki, N. F. T. Aniceto, H. Karvonen, I. Vidal, F. Valera, P. A. S. M. Barreto, M. F. Caetano, W. D. Dias, and G. Fettweis, "Enhanced Remote Areas Communications: The Missing Scenario for 5G and Beyond 5G Networks," *IEEE Access*, vol. 8, pp. 219 859–219 880, 2020.

[3] "Measuring digital development: Facts & figures 2019," https://www.itu.int/en/myitu/News/2020/05/25/16/23/Measuring-digital-development-Facts--figures-2019, accessed: 2020-10-10.

[4] R. Bahrini and A. A. Qaffas, "Impact of information and communication technology on economic growth: Evidence from developing countries," *Economies*, vol. 7, no. 1, p. 21, 2019.

[5] C. Choi and M. H. Yi, "The effect of the Internet on economic growth: Evidence from cross-country panel data," *Economics Letters*, vol. 105, no. 1, pp. 39–41, 2009.

[6] L. Nagpal and K. Samdani, "Project Loon: Innovating the connectivity worldwide," in *2017 2nd IEEE International Conference on Recent Trends in Electronics, Information & Communication Technology (RTEICT)*. IEEE, 2017, pp. 1778–1784.

[7] W. Dias, D. Gaspar, L. Mendes, M. Chafii, M. Matthé, P. Neuhaus, and G. Fettweis, "Performance Analysis of a 5G Transceiver Implementation for Remote Areas Scenarios," in *2018 European Conference on Networks and Communications (EuCNC)*, 2018, pp. 363–367.

[8] A. Ferreira, L. Mendes, W. Dias, T. Marins, D. Gaspar, A. Matos, C. Silva, and B. Sokal, "5G-RANGE Project Field Trial," in *2019 European Conference on Networks and Communications (EuCNC)*, 2019, pp. 490–494.

[9] I. Gaspar, N. Michailow, A. Navarro, E. Ohlmer, S. Krone, and G. Fettweis, "Low complexity GFDM receiver based on sparse frequency domain processing," in *Vehicular Technology Conference (VTC Spring), 2013 IEEE 77th*. IEEE, 2013, pp. 1–6.

[10] A. Farhang, N. Marchetti, and L. E. Doyle, "Low-Complexity Modem Design for GFDM." *IEEE Trans. Signal Processing*, vol. 64, no. 6, pp. 1507–1518, 2016.

[11] M. Matthe, I. Gaspar, D. Zhang, and G. Fettweis, "Reduced complexity calculation of LMMSE filter coefficients for GFDM," in *Vehicular Technology Conference (VTC Fall), 2015 IEEE 82nd*. IEEE, 2015, pp. 1–2.

[12] P. Wei, X.-G. Xia, Y. Xiao, and S. Li, "Fast dgt-based receivers for gfdm in broadband channels," *IEEE Trans. on Communications*, vol. 64, no. 10, pp. 4331–4345, 2016.

[13] P.-C. Chen, B. Su, and Y. Huang, "Matrix characterization for gfdm: low complexity mmse receivers and optimal filters," *IEEE Trans. on Signal Processing*, vol. 65, no. 18, pp. 4940–4955, 2017.

[14] J. Mitola and G. Q. Maguire, "Cognitive radio: making software radios more personal," *IEEE Personal Commun. Mag.*, vol. 6, no. 4, pp. 13–18, 1999.

[15] A. Achtzehn, L. Simić, M. Petrova, and P. Mähönen, "Feasibility of Secondary Networks: Analysis Methodology and Quantitative Study of Cellular and Wi-Fi-Like TVWS Deployments," *IEEE Transactions on Mobile Computing*, vol. 14, no. 2, pp. 373–386, 2015.

[16] Farhang-Boroujeny, Behrouz and Moradi, Hussein, "OFDM inspired waveforms for 5G," *IEEE Communications Surveys & Tutorials*, vol. 18, no. 4, pp. 2474–2492, 2016.

[17] K. R. Rao and P. C. Yip, *The transform and data compression handbook*. CRC press, 2000.

[18] Baltar, Leonardo G and Waldhauser, Dirk S and Nossek, Josef A, "Out-of-band radiation in multicarrier systems: a comparison," in *Multi-Carrier Spread Spectrum 2007*. Springer, 2007, pp. 107–116.

[19] Abdoli, Javad and Jia, Ming and Ma, Jianglei, "Filtered OFDM: A new waveform for future wireless systems," in *2015 IEEE 16th International Workshop on Signal Processing Advances in Wireless Communications (SPAWC)*. IEEE, 2015, pp. 66–70.

[20] K. Mizutani and H. Harada, "Universal time-domain windowed OFDM," in *2016 IEEE 84th Vehicular Technology Conference (VTC-Fall)*. IEEE, 2016, pp. 1–5.

[21] L. Mendes, N. Michailow, M. Matthé, I. Gaspar, D. Zhang, and G. Fettweis, "GFDM: Providing Flexibility for the 5G Physical Layer," in *Opportunities in 5G Networks: A Research and Development Perspective*. CRC Press, 2016, pp. 325–390.

[22] N. Michailow, M. Matthé, I. S. Gaspar, A. N. Caldevilla, L. L. Mendes, A. Festag, and G. Fettweis, "Generalized frequency division multiplexing for 5th generation cellular networks," *IEEE Trans. on Communications*, vol. 62, no. 9, pp. 3045–3061, 2014.

[23] J. W. Cooley and J. W. Tukey, "An algorithm for the machine calculation of complex Fourier series," *Mathematics of computation*, vol. 19, no. 90, pp. 297–301, 1965.

[24] M. Matthé, L. Mendes, I. Gaspar, N. Michailow, D. Zhang, and G. Fettweis, "Precoded GFDM transceiver with low complexity time domain processing," *EURASIP Journal on Wireless Communications and Networking*, vol. 2016,

no. 1, p. 138, 2016.

[25] S. M. Alamouti, "A simple transmit diversity technique for wireless communications," *IEEE Journal on selected areas in communications*, vol. 16, no. 8, pp. 1451–1458, 1998.

[26] N. Al-Dhahir, "Single-carrier frequency-domain equalization for space-time block-coded transmissions over frequency-selective fading channels," *IEEE Communications Letters*, vol. 5, no. 7, pp. 304–306, 2001.

[27] M. Matthe, L. L. Mendes, I. Gaspar, N. Michailow, D. Zhang, and G. Fettweis, "Multi-user time-reversal STC-GFDMA for future wireless networks," *EURASIP Journal on Wireless Communications and Networking*, vol. 2015, no. 1, pp. 1–8, 2015.

[28] S. M. Kay, *Fundamentals of statistical signal processing: Detection theory*. Prentice Hall PTR, 1993.

[29] C. Candan. (2011) Notes on Linear Minimum Mean Square Error Estimators. [Online]. Available: https://users.metu.edu.tr/ccandan/ee503/ee503_fall201011/lecture_notes/linear_mmse_notes.pdf

[30] L. G. Baltar, A. Mezghani, and J. A. Nossek, "MLSE and MMSE subchannel equalization for filter bank based multicarrier systems: Coded and uncoded results," in *2010 18th European Signal Processing Conference*. IEEE, 2010, pp. 2186–2190.

[31] J. Cioffi, G. Dudevoir, M. Eyuboglu, and G. Forney, "Minimum mean-square-error decision feedback equalization and coding-parts I and II," *IEEE Trans. Commun.*, vol. 43, no. 10, pp. 2582–2604, 1995.

[32] ITU-T, "Report BT.2035 : Guidelines and techniques for the evaluation of digital terrestrial television broadcasting systems including assessment of their coverage areas," ITU-T, Tech. Rep., 2008.

[33] Vodafone Chair For Mobile Communications Systems TU Dresden. (2020) "Generalized Frequency Division Multiplexing (GFDM) library for MATLAB". [Online]. Available: https://github.com/vodafone-chair/gfdm-lib-matlab

[34] W. Dias, A. Ferreira, R. Kagami, J. S. Ferreira, D. Silva, and L. Mendes, "5G-RANGE: A transceiver for remote areas based on software-defined radio," in *2020 European Conference on Networks and Communications (EuCNC)*, 2020, pp. 100–104.

[35] M. Frigo and S. G. Johnson, "FFTW: An adaptive software architecture for the FFT," in *Proceedings of the 1998 IEEE International Conference on Acoustics, Speech and Signal Processing, ICASSP'98 (Cat. No. 98CH36181)*, vol. 3. IEEE, 1998, pp. 1381–1384.

[36] The GNU Project. (2021) GCC, the GNU Compiler Collection. [Online]. Available: https://gcc.gnu.org

[37] M. Klemm, A. Duran, X. Tian, H. Saito, D. Caballero, and X. Martorell, "Extending OpenMP with vector constructs for modern multicore SIMD architectures," in *International Workshop on OpenMP*. Springer, 2012, pp. 59–72.

[38] Google. (2013) Google benchmark: A library to benchmark code snippets. [Online]. Available: https://github.com/google/benchmark

[39] G. Surabhi and A. Chockalingam, "Low-complexity linear equalization for OTFS modulation," *IEEE Communications Letters*, vol. 24, no. 2, pp. 330–334, 2019.